Role of the NLRP3 inflammasome in bone marrow fibrosis, neural damage, and mesenchymal stem cell survival in Myeloproliferative Neoplasms

Doctoral thesis

to obtain a doctorate (Dr. med.)

from the Faculty of Medicine

of the University of Bonn

Elisabeth Rosina Ursula Tregel

from Munich

2025

Written with authorization of

the Faculty of Medicine of the University of Bonn

First reviewer: Prof. Dr. Peter Brossart

Second reviewer: PD Dr. Christian Jansen

Day of oral examination: 22.09.2025

From the Clinic and Polyclinic for Hematology-Oncology, Immuno-oncology, and Rheumatology

Table of contents

List of abbreviations

Adrb3	β3-adrenergic receptor
allo-HSCT	Allogeneic hematopoietic stem cell transplantation
ALR	Absent in melanoma 2-like receptor
ANOVA	Analysis of Variance
APC	Antigen presenting cell
ASC	Apoptosis-associated speck-like protein containing a CARD
ATP	Adenosine Triphosphate
BM	Bone marrow
CALR	Calreticulin
CARD	Caspase recruiting domain
CD	Cluster of Differentiation
cDNA	complementary DNA
CEL	Chronic eosinophilic leukemia
cGAS	Cyclic GMP-AMP synthase
CLP	Common Lymphoid Progenitor
CLR	C-type lectin receptor
CML	Chronic myeloid leukemia
CMML	Chronic Myelomonocytic Leukemia
CMP	Common Myeloid Progenitor
CNL	Chronic neutrophilic leukemia
CO_2	Carbon dioxide
COL1A1	Collagen Type I Alpha 1 Chain
DAMP	Damage associated molecular pattern
DMSO	Dimethyl sulfoxide
DNA	Deoxyribonucleic acid, Desoxyribonucleic Acid
dNTP	Deoxynucleotide triphospate
DPBS	Dulbecco's Phosphate-buffered Saline
EC	Endothelial cell

ECM	Extracellular Matrix
EDTA	EthylenDiamin TetraAcetic Acid
ER	Endoplasmic reticulum
ErP	Erythrocyte Precursor
ET	Essential thrombocythemia
EV	Empty vector
FCS	Fetal Calf Serum
FIJI	Fiji Is Just ImageJ
GAPDH	Glyeraldehyde 3-phosphate dehydrogenase
GFAP	Glial Fibrillary Acidic Protein
GMP	Granulocyte-Macrophage Progenitor
GSDMD	Gasdermin D
H&E	Hematoxylin & Eosin
H_2O_2	Hydrogen Peroxide
HET	House of Experimental Therapies
HPF	High-power field
HRP	Horseradish Peroxidase
HSC	Hematopoietic Stem Cell
ICC	International Consensus Classification
IHC	Immunohistochemistry
IL-1β	Interleukin-1 Beta
IVC	Individually ventilated cages
JAK2	Janus kinase 2
JMML	Juvenile myelomonocytic leukemia
LRR	Leucine-rich repeats
MDS	Myelodysplatic Syndrome
MF	Myelofibrosis
MkP	Megakaryocyte Percursor
MPL	Myeloproliferative leukemia virus oncogene
MPN	Myeloproliferative Neoplasm
MPN-BP	Myeloproliferative neoplasm - Blast phase
MPN-NOS	Myeloproliferative neoplasm - not other specified

MPP	Multipotent Progenitor
mRNA	messenger RNA
MSC	Mesenchymal stem cell
NCBI	National Center for Biotechnology Information
NF-kB	Nuclear factor kappa-light-chain-enhancer of activated B cells
NK	Natural killer
NLR	NOD like receptor
NLRP	NLR family pyrin domain
NLRP3	NLR family pyrin domain containing 3
NOD	Nucleotide-binding and oligomerization domain
PAMP	Pathogen associated molecular pattern
PB	Peripheral blood
PCR	Polymerase Chain Reaction
PEG-IFNα	Pegylated Interferon-alpha
PFA	Paraformaldehyde
PMF	Primary myelofibrosis
PRR	Pattern recognition receptor
PV	Polycythemia vera
PYD	Pyrin domain
RFU	Relative Fluorescence Unit
RLR	Retinoid acid-inducible gene-I-like receptor
RLU	Relative Luminescence Unit
RNA	Ribonucleic acid
ROS	Reactive oxygen species
RPMI	Roswell Park Memorial Institute Medium
RT	Room temperature
RT-qPCR	Real-time quantitative polymerase chain reaction
SEM	Statistical Error of the Mean
sMF	Secondary Myelofibrosis
SPF	Specific pathogen-free
TBS	Tris-Buffered Saline

TGF-β	Transforming Growth Factor Beta
TH	Tyrosine Hydroxylase
TLR	Toll-like receptor
TNFα	Tumor Necrosis Factor Alpha
TPO	Thrombopoietin
WHO	World Health Organization
WT	Wildtype
ΔΔCt	Delta-delta Ct

1. Introduction

1.1 Hematopoiesis

Hematopoiesis is the dynamic and highly regulated process of blood cell formation, development, and maturation. In human development, hematopoiesis begins in the yolk sac during embryonic stage. It then transitions temporarily to the liver before moving to the thymus and bone marrow (BM) (Tavian et al., 2010). In adults, hematopoiesis occurs in the bone marrow mainly in the cranium, pelvis, sternum, and vertebrae (Fernández and de Alarcón, 2013). When there is medullary insufficiency or hematopoietic stress, the liver and spleen can take over the role of hematopoiesis, a phenomenon referred to as extramedullary hematopoiesis (Kim, 2010). Hematopoiesis follows a hierarchical organization, starting with hematopoietic stem cells (HSCs) (Zhang et al., 2018), (see Figure 1). Among other factors, the maintenance, proliferation, and maturation of HSCs is regulated by the bone marrow microenvironment providing different niches (Lucas, 2021). HSCs have the unique ability to self-renew and differentiate into different progenitor cell populations, ultimately leading to the production of mature blood cells (Zon, 2008). The four major lineages are erythropoiesis, megakaryocytopoiesis, myelopoiesis and lymphopoiesis resulting in the production of erythrocytes, thrombocytes, monocytes, granulocytes, and lymphocytes. These cells have distinct functions in oxygen transport, blood clotting and immune response (Pucella et al., 2020).

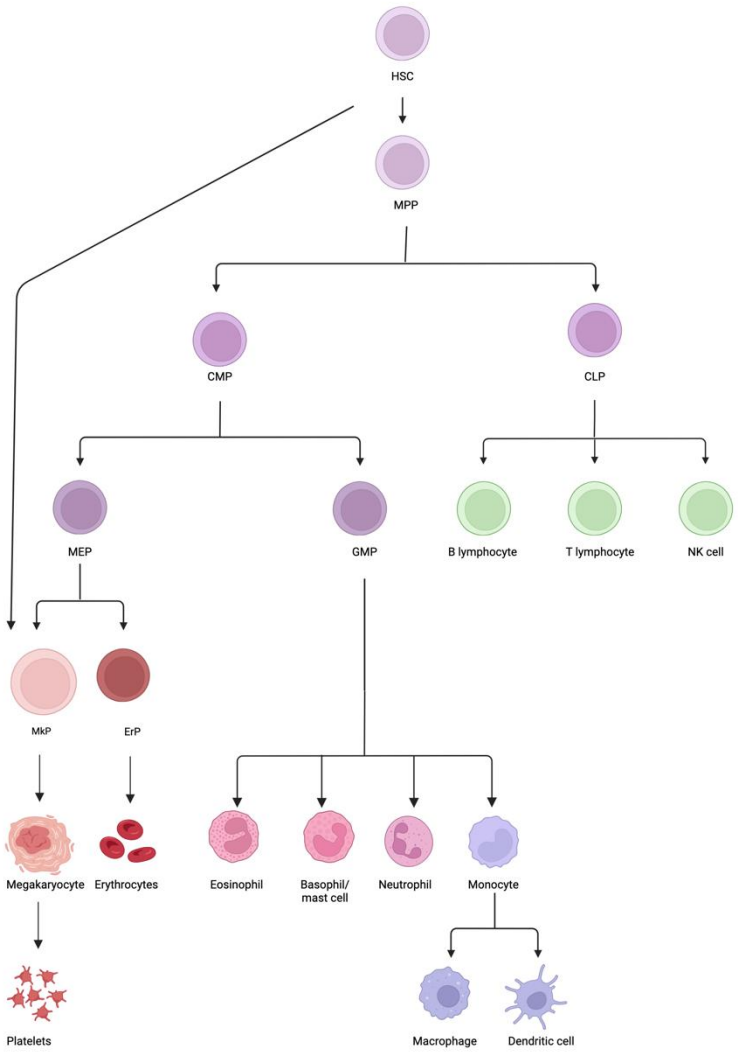

Figure 1: Schematic hierarchy of hematopoiesis

Hematopoietic stem cells (HSC) are at the origin of hematopoiesis and differentiate into multipotent progenitor (MPP) cells. Downstream, common myeloid progenitor (CMP) and common lymphoid progenitor (CLP) give rise to the myeloid and lymphoid lineages, respectively. HSC can also give rise directly to megakaryocyte precursors (MkP) (Morcos et al., 2022). From CMP, erythrocyte precursors (ErP) and MkP differentiate into erythrocytes, megakaryocytes, and thrombocytes. Granulocyte-macrophage progenitors (GMP), derived from CMP, give rise to granulocytes (eosinophils, basophils/mast cells, and neutrophils) and monocytes, which differentiate into macrophages and dendritic cells. Mature blood cells of the lymphoid lineage include T lymphocytes, B lymphocytes, natural killer (NK) cells, and dendritic cells. (Zhang et al., 2018), modified by author. Created with BioRender.com.

Enhancing comprehension of hematopoiesis and elucidating the regulatory mechanisms governing HSCs in a state of homeostasis can provide valuable insights into alterations observed in clonal hematopoietic disorders.

1.2 MPN

Myeloproliferative Neoplasms (MPN) are stem cell-derived clonal bone marrow disorders in which the acquisition of somatic mutations promotes clonal expansion and myeloid differentiation (Zoi and Cross, 2017). These malignant hematologic disorders occur with a cumulative incidence of 5-10 / 100.000 per year (Anderson and McMullin, 2014). The World Health Organization (WHO) classifies eight subtypes of MPN: chronic myeloid leukemia (CML), polycythaemia vera (PV), essential thrombocythemia (ET), primary myelofibrosis (PMF), chronic neutrophilic leukemia (CNL), chronic eosinophilic leukemia (CEL), juvenile myelomonocytic leukemia (JMML) and myeloproliferative neoplasm, not other specified (MPN-NOS) (Khoury et al., 2022). The diagnostic hallmark of CML is the BCR-ABL1 fusion gene, a reciprocal translocation between chromosomes 9 and 22, also known as the Philadelphia chromosome (Kurzrock et al., 2003). Classical BCR-ABL1-negative MPNs are PV, ET and PMF (Zoi and Cross, 2017). These MPNs are instigated by driver mutations in the genes encoding Janus kinase 2 (*JAK2*), calreticulin (*CALR*) and thrombopoietin (TPO) receptor, encoded by the myeloproliferative leukemia virus oncogene (*MPL*) (Kim et al., 2015). The gain-of-function *JAK2*V617F mutation is most common, occurring in 95 % of patients suffering from PV and in 50-60 % persons diagnosed with ET or PMF (Szybinski and Meyer, 2021). The *JAK2*V617F mutation leads to constitutive activation of JAK2 and its downstream signaling pathways, resulting in promotion of myeloid cell proliferation and cell survival (Bader and Meyer, 2022).

MPLW515L is the most prevalent *MPL* mutation and occurs in 3-15 % of cases of ET and PMF. It constitutively activates the TPO receptor through JAK2 signaling (Tefferi, 2010). Calreticulin serves as a chaperone in the endoplasmic reticulum (ER) and facilitates calcium binding. The most common CALR Exon 9 mutations are CALR-deletion52 and CALR-insertion5, which interfere with the ER retention signal. At the cell surface the changed protein structure associates with MPL and leads to aberrant MPL-JAK2 pathway activation (Szybinski and Meyer, 2021). CALR mutations are found in approximately 20.8 % cases of ET and in 30.8 % PMF patients (Klampfl et al., 2013). In 10-15 % of ET

and PMF patients none of these three major driver mutations can be detected and they are therefore called “triple negative” MPN (Langabeer, 2016).

For the correct MPN subtype diagnosis the WHO proposes the evaluation of “clinical features, peripheral blood counts and smear analysis, BM morphology, karyotype, and molecular genetic tests” (Kvasnicka, 2019). BM changes are determined by proliferation of one or more myeloid lineages with megakaryocytic hyperplasia occurring in the BM of all BCR-ABL1-negative MPN (Hoffman et al., 2007). Major criteria for the diagnosis of PV are increased erythrocyte counts with consistent BM findings, while ET is associated with elevated platelets and megakaryocytic hyperplasia (Pizzi et al., 2021). PMF is subclassified by the International Consensus Classification (ICC) into an overly fibrotic stage and a pre-fibrotic/early stage, characterized by increased atypical megakaryocytes and mild (pre-fibrotic phase) to severe (fibrotic phase) fibrosis grade (Tefferi, 2023).

Common symptoms across all three MPNs include abdominal discomfort (mostly caused by splenomegaly), fatigue, night sweats, bone pain, fever, weight loss and other symptoms (Scherber et al., 2011). During disease progression, MPN patients may suffer from suppression of normal hematopoiesis, total bone marrow failure and secondary leukemic transformation into MPN blast phase (MPN-BP) defined by >20 % blasts in peripheral blood (PB) or BM (Baumeister et al., 2021). Apart from the transformation in acute leukemia, PV and ET can progress into secondary MF (sMF) referred to as post-ET-MF or post-PV-MF. Myelofibrosis is characterized by fibrotic remodeling in the BM, increased proliferation and size of megakaryocytes and eventually extramedullary hematopoiesis (Gangat und Tefferi, 2020). The risk of MPN patients to develop thrombotic and hemorrhagic complications increases morbidity and, potentially, mortality (Baumeister et al, 2021; Curto-Garcia et al., 2020). Median survival times are dependent on the MPN subtype and spread from few months to years. While life expectancy is nearly normal in ET patients (median survival time of 19.8 years), it is impaired in PV (13.5 years) and worst in PMF (5.9 years) and triple negative PMF (2.3 years) patients (Tefferi et al., 2014). In MPN-BP survival is immensely reduced (median overall survival of 2.6 months) (Tallarico and Odenike, 2015).

Current treatments in BCR-ABL-negative MPN have improved and can ameliorate clinical symptoms. However, they lack to cure MPN. For cytoreductive therapy, both hydroxyurea

and anagrelide can be used in ET, while in PV, hydroxyurea is utilized to prevent thrombotic events (Baumeister et al., 2021). In MF the JAK1/JAK2 inhibitor Ruxolitinib successfully reduces splenomegaly and MF-associated symptoms (Harrison et al., 2012). Still, it is important to note that many patients experience a loss of response during therapy with a 48 % probability of maintaining response at the 5-year mark (Harrison et al., 2016). Pegylated Interferon-alpha (PEG-IFNα) is reported to induce hematologic and molecular response in ET and PV (Quintás-Cardama et al., 2013; Stegelmann et al., 2023). Sole curative therapy for advanced MF is allogeneic hematopoietic stem cell transplantation (allo-HSCT), but as this intense treatment is only an option for patients with a good performance status, it cannot be applied in most patients (Kröger et al., 2015). Therefore, novel curative therapeutic options must be approached to prevent disease progression.

1.3 Inflammation and the BM microenvironment

The dynamic BM microenvironment plays an important role in normal and disease state. This niche is a tight network of cell interactions that regulates proliferation, differentiation, localization, and self-renewal during physiological homeostasis. It consists of individual compartments as the endosteal niche, the vascular niche, sympathetic nervous system, and extracellular matrix (ECM), which form the microenvironment for HSCs (Curto-Garcia et al., 2020). Irregularities in all niches have been described as potentially causative for MPN disease dynamics (Behrmann et al., 2020), (see Figure 2).

The endosteal niche consists of osteoblast, osteoclast, and spindle-shaped N-cadherin+ osteoblast cells, which ensure maintenance, proliferation, and differentiation of HSCs (Curto-Garcia et al., 2020). However, in MPN this osteoblast-osteoclast axis is disrupted. An abnormal expansion of osteoblast promotes fibrogenesis and overproduction of inflammatory cytokines resulting in osteosclerosis while osteoclasts favor survival of HSC (Curto-Garcia et al., 2020; Schepers et al., 2013).

The vascular niche is formed by blood vessels, endothelial cells (EC), stromal elements, fibronectin, and collagen, important for HSC dormancy, expansion, and migration (Curto-Garcia et al., 2020). When disrupted, proliferation of ECs is stimulated by leukemic cells, which produce angiogenic factors and inflammatory cytokines (e.g., Tumor Necrosis Factor Alpha (TNFα) and Interleukin-1 Beta (IL-1β)) leading to neo-angiogenesis and fibrosis (Korn and Méndez-Ferrer, 2017).

BM nestin^{+} mesenchymal stem cells (MSC) are multipotent cells encompassing cartilage, bone and adipose tissue and play a pertinent role in HSC maintenance (García-García et al., 2015). MSCs are responsible for the MPN phenotype as deregulated growth and differentiation of MSCs results in BM fibrosis mediated through increased production of Transforming Growth Factor Beta (TGF-β), IL-1β, and other cytokines (Schepers et al., 2015).

MSCs in turn are innervated by sympathetic nerve fibers, which regulate HSC traffic via β-3-adrenergic receptor activation in MSCs (Méndez-Ferrer et al., 2008). In MPN a local neuropathy, meaning loss of sympathetic nerve fibers and supporting Schwann cells, can be observed due to increased IL-1β production by mutant HSCs (Arranz et al., 2014). This neuroglial damage compromises MSC survival, which again leads to MPN progression (Arranz et al., 2014). β-3-adrenergic receptor reveals a protective role as its activation plays an indispensably role in regulation of HSC functionality and egress (Arranz et al., 2014).

The ECM as a non-cellular space helps to maintain HSCs with growth factors and is important for proliferation, integrity and dynamic in the BM niche. As mutant HSCs secrete increased levels of cytokines and growth factors within the ECM, disease progression and maintenance is perturbed (Curto-Garcia et al., 2020). TGFβ, a fibrogenic cytokine, promotes fibrosis by promoting MSC differentiation towards fibroblasts and osteoblasts accompanied by an increased production of collagen (Curto-Garcia et al., 2020).

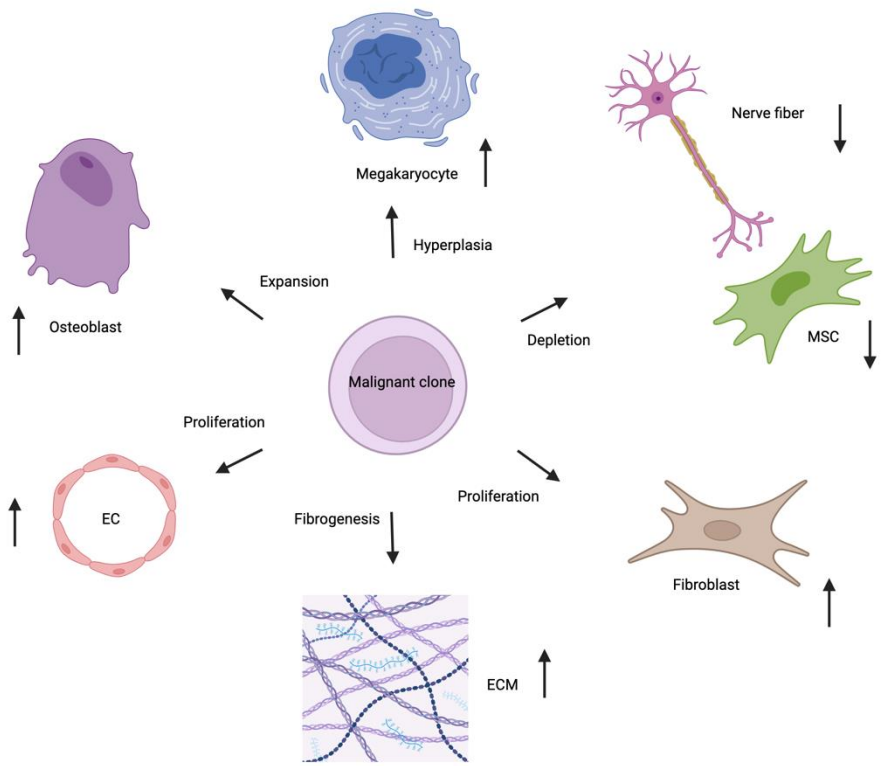

Figure 2: Overview of the bone marrow niche

Different cell types are involved in regulating HSCs. In MPN neural damage results in loss of MSC while other cell populations expand abnormally. HSC, hematopoietic stem cell, MSC, mesenchymal stem cell, ECM, extracellular matrix, EC, endothelial cell. (Behrmann et al., 2020), modified by author. Created with BioRender.com.

This tight interplay between clonal and non-clonal cells shows that both malignant and nonmalignant cells contribute to the MPN phenotype (Koschmieder et al., 2016). It is known that the constitutive activation of the JAK/STAT pathway by gene mutations triggers cytokine production in malignant and nonmalignant cells, which leads to disease development and progression (Kleppe et al., 2015). MPN-associated inflammation is mirrored by upregulated pro-inflammatory cytokines like TNFα and IL-1β, which lead to MPN defining events. Dysregulated IL-1β production leads to BM neuropathy causing MSC cell death and therefore promoting fibrosis and altered hematopoiesis in MPN (Arranz et al., 2014). Additionally, myelofibrosis is driven by increased levels of IL-1β and hyperplastic megakaryocytes, which release profibrotic factors (Rai et al., 2022).

Following this, the persistent inflammatory condition is apt to trigger and sustain the ailment by influencing the nonclonal microenvironment, thereby promoting the expansion of the malignant clone and inhibiting regular hematopoiesis (Koschmieder et al., 2016). Nevertheless, it remains unclear whether the inflammation primarily stems from the malignant clone or if the malignant clone merely induces a self-sustaining chronic inflammatory reaction in the nonclonal hematopoietic microenvironment, fostering further clonal proliferation.

Examining the BM microenvironment with a focus on the impact of the NLRP3 inflammasome in MPN seeks to elucidate the underlying mechanisms driving disease progression. A complete understanding of the origins of inflammation necessitated a thorough examination of key contributors that initiate and perpetuate inflammatory states. Foremost among these contributors are inflammasomes, pivotal in the regulation of cytokine production.

1.4 NLRP3 inflammasome

The immune system consists of the innate and adaptive immune system (Chaplin, 2010). The native immune system is the first line of host defense by recognizing harmful stimuli such as pathogens, tissue damage or stress (Chaplin, 2010). Pathogen-associated molecular patterns (PAMPs) and damage associated molecular patterns (DAMPs) are detected by pattern recognition receptors (PRRs), the sensor proteins of inflammasomes, which are expressed by cells of the innate immune system, e.g., antigen presenting cells, APCs (Kelley et al., 2019). The following PRR families are known: toll-like receptors (TLRs) and C-type lectin receptors (CLRs), retinoic acid-inducible gene, RIG-I-like receptor (RLRs), absent in melanoma 2, AIM2-like receptor (ALRs), nucleotide-binding and oligomerization (NOD) domain like receptors (NLRs) and cytosolic sensor cyclic GMP-AMP synthase (cGAS) (Moossavi et al., 2018). NLRs are cytosolic proteins and have different domains. A main nucleotide binding and oligomerization domain, NOD, a C-terminal with leucine-rich repeats (LRR) and a N-terminal domain (Moossavi et al., 2018). Depending on the N-terminal domain, NLRs are subcategorized and NLRs containing a pyrin domain (PYD) are therefore called NLRP (Moossavi et al., 2018). Some types of NLRs (e.g., NLRP1 and NLRP3) can oligomerize forming large multimeric protein complexes, which are called inflammasomes (Moossavi et al., 2018). Once activated inflammasomes trigger

the release of proinflammatory cytokines representing a significant inflammatory pathway (Blevins et al., 2022). This renders them a compelling subject for exploration.

NLRP3 is one of the most described inflammasomes and reacts to a wide range of PAMPs and DAMPs (Kelley et al., 2019). The NLRP3 scaffold (sensor) forms the NLRP3 inflammasome complex together with the apoptosis-associated speck-like protein containing a caspase recruiting domain (CARD), ASC (adaptor) and capase-1 (effector) (Moossavi et al., 2018). Many stimuli can activate the NLRP3 inflammasome via a two-signal model, consisting of a priming and activation signal (Tartey and Kanneganti, 2019), (see Figure 3). Signal 1 induces the nuclear factor kappa-light-chain-enhancer of activated B cells (NF-kB) signaling cascade triggered by PAMPs and DAMPs. NF-kB translocates to the nucleus, leading to the transcription of pro-Interleukin-1 beta (pro-IL-1β) and pro-Interleukin-18 (pro-IL-18) (Tartey and Kanneganti, 2019). Involving pore-forming toxins and particulates, the activation signal (signal 2) induces the oligomerization of NLRP3 and assembly of the inflammasome complex. Pore-forming toxins and particulates trigger ionic flux, activating NLRP3. Additionally, mitochondrial degradation, reactive oxygen species (ROS) and extracellular Adenosine Triphosphate (ATP) contribute to NLRP3 activation (Kelley et al., 2019). Ultimately, these signals culminate the activation of pro-Caspase-1 via the ASC domain (Moossavi et al., 2018). Activated caspase-1 then processes pro-IL-1β, pro-IL-18 and gasdermin D (GSDMD) into active forms (Kelley et al., 2019). IL-1β effects various physiological processes, such as inducing fever and inflammatory pain hypersensitivity and affecting endothelial cells while IL-18 promotes interferon-gamma production (Martinon and Tschopp, 2007). Additionally, active GSDMD mediates caspase-1-induced inflammatory cell death, also referred to as pyroptosis, causing plasma-membrane rupture and further supporting cytokine release (Kelley et al., 2019). NLRP3 activation has been described to be involved in tumorigenesis of lung cancer, melanoma, breast cancer and others (Moossavi et al., 2018).

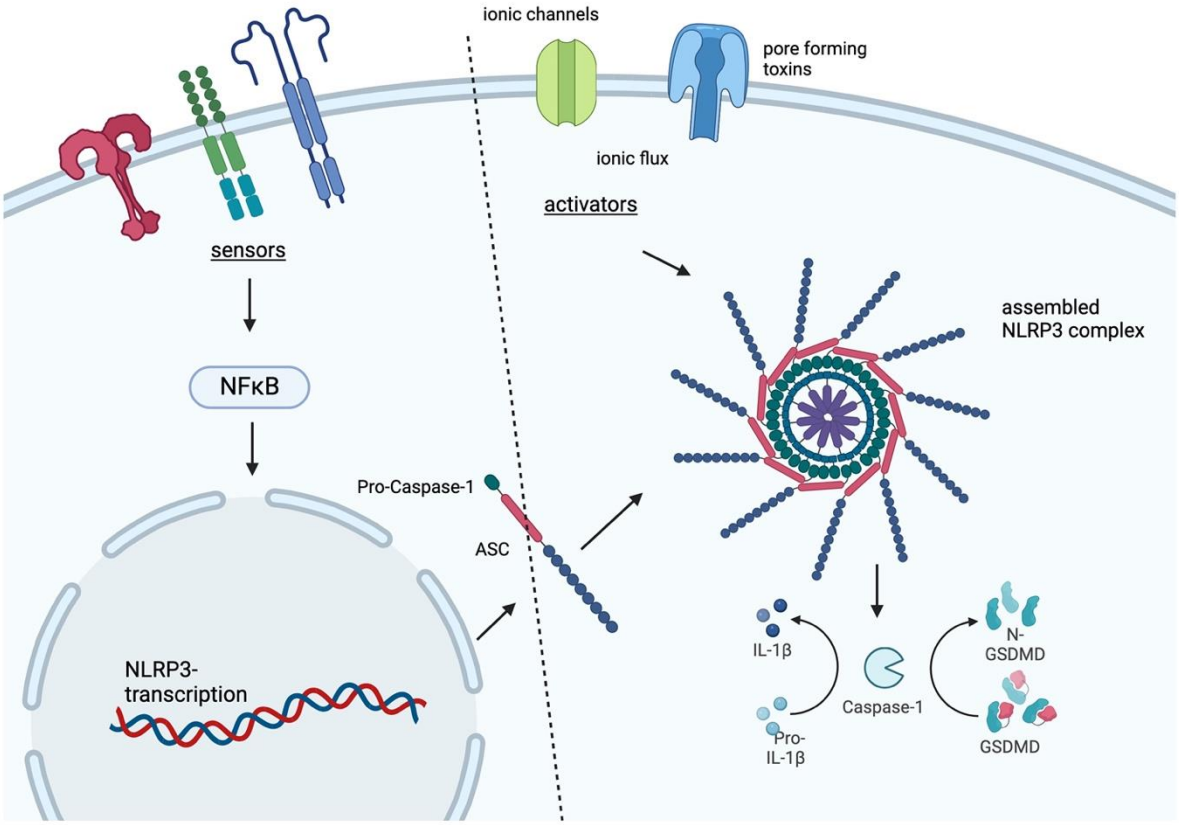

Figure 3: Activation mechanism of the NLRP3 inflammasome

Signal 1 (left) involves the induction of NF-kB signaling cascade triggered by TLRs, NLRs and cytokine receptors at the cell surface. The activation signal (signal 2, right) involves the assembly of the inflammasome complex triggered by activators (e.g. ionic flux) activating pro-Caspase-1, which leads to the processing of pro-cytokines into their active forms. ASC, apoptosis-associated speck-like protein, NFkB, nuclear factor-kB, GSDMD, gasdermin D. (Kelley et al., 2019), modified by author. Created with BioRender.com.

Scrutinizing the influence of the NLRP3 inflammasome in the pathobiology of MPN holds promise for advancing our comprehension of disease progression and exploring their potential therapeutic efficiency in these malignancies. Against this background finding specific therapeutic targets that promote disease initiation and progression is one key goal of therapeutic intervention.

1.5 Aim of the thesis

The aim of this thesis was to evaluate the role of the NLRP3 inflammasome in driving inflammation in classical BCR-ABL-negative MPN. To meet the study's objective a three-step experimental design was proposed.

Aim 1: Analyze if inflammasome activation occurs in MPN

To assess inflammasome activation in MPN, a murine cell line with the following mutations, *JAK2V617F*, *CALR-del52,* or *CALR-ins5,* and a WT control were analyzed. To test whether the NLRP3 inflammasome is activated in MPN, Caspase-1 activity and ROS production were measured via luminescence and fluorescence in these cells.

Aim 2: Investigate if *Nlrp3* deficiency leads to less bone marrow fibrosis and regulation of excess megakaryopoiesis in MPN

The inflammatory state in MPN is supposed to be a major driver of myelofibrosis and excess megakaryopoiesis (see chapter 1.3). To determine the role of NLRP3, a murine *Jak2*^{VF} MPN model with a wildtype *Nlrp3* and a homozygous *Nlrp3* knout-out gene was used. The grade of fibrosis depending on the presence of *Nlrp3* was determined by analyzing BM and spleen sections stained for reticular fibers of *Jak2*^{VF} and *Jak2*^{VF}*;Nlrp3*$^{-/-}$ mice. Additionally, the expression level of the gene for Collagen Type I Alpha 1 Chain (*COL1A1*), (a marker for fibrosis) in BM cells of each line was analyzed by Real-Time Quantitative Polymerase Chain Reaction (RT-qPCR). Effects of NLRP3 on megakaryopoiesis were evaluated by exanimating number and size of megakaryocytes in BM and spleen sections of each line.

Aim 3: Determine whether *Nlrp3* deficiency in MPN reduces neuroglial damage and promotes MSC survival

As described above, the NLRP3 inflammasome is a key source of IL-1β activation. *Jak2*^{VF} mutated HSCs promote IL-1β driven inflammation causing neuroglial damage and MSC loss as they are innervated by sympathetic nerve fibers. BM sections of *Jak2*^{VF} and *Jak2*^{VF}*;Nlrp3*$^{-/-}$ mice were examined by Immunohistochemistry (IHC) staining for sympathetic nerve fibers, Schwann cells and MSCs to investigate the effects of IL-1β driven

neuropathy and MSC loss. Alterations in the expression level of the gene coding for the β3-adrenergic receptor (*Adrb3*) were analyzed by RT-qPCR.

2 Materials, mice, and methods

2.1 Materials

2.1.1 Equipment

Table 1: Equipment

Item	Model	Supplier
Cell counting chamber	Neubauer	Brand, Wertheim, Germany
Centrifuge	5430, 230V/50-60Hz	Eppendorf, Hamburg, Germany
Fluorescence reader	SpectraMax i3 Multi-Mode Detection Platform	Molecular Devices, LL, San José, USA
Freezer (-20 °C)	SRFfg 3501	Liebherr, Bulle, Switzerland
Freezer (-80 °C)	Forma 900 Series 5908	Thermo Fisher Scientific, Waltham, USA
Freezer (-150 °C)		SANYO Biomedical, Moriguchi, Japan
Fridge (+4 °C)	SRFfg 3501	Liebherr
Heatblock Thermomixer	Thermomixer comfort 24 x 1.5 ml	Eppendorf
Incubator	Galaxy 170 R/S	Eppendorf
Laminar airflow Workbench	Hera safe	Thermo Fisher Scientific
Luminescence reader	GloMax Discover Microplate Reader	Promega, Fitchburg, USA

Microscope for plates	E-200	Nikon, Düsseldorf, Germany
Microscope for slides	TS-100	Nikon
Microscope for imaging	BX51	Olympus, Tokio, Japan
Microtome	SM2010 R	Leica Biosystems, Wetzlar, Germany
Freezing container	Mr. Frosty™	Thermo Fisher Scientific
Pipetting aid	Pipetboy acu 2	Integra, Zizers, Switzerland
Plate shaker	Thermal Mixer	Thermo Fisher Scientific
qPCR cycler	Mastercycler realplex^2	Eppendorf
RNA isolation	Maxwell® CSC 48	Promega
Scale	PR Analytical	Ohaus Cooperation, Parsippany, USA
Single channel pipettes	Eppendorf Research	Eppendorf
Spectrophotometer	NanoDrop 2000/2000c	Thermo Fisher Scientific
Steam cooker	19270-56	Spectrum Brands, Madison, Wisconsin, USA
Vetenary Haematology Analyser	BC-500	Mindray, Shenzhen, China
Vortex mixer	MX-S	Biologix, Hallbergmoos, Germany
Water bath	WNB 22	Memmert, Schwabach, Germany

2.1.2 Consumables

Table 2: Consumables

Item	Supplier
Cell culture plates (96-well)	Becton Dickinson, Franklin Lakes, USA
Cell culture flasks (25 and 75 cm^2)	Corning, New York, USA
Cell strainer metal	Feinwerkstatt Bonn University, Germany
Coverslips	Marienfeld, Lauda-Königshofen, Germany
Filter tips (0.1 – 1 ml)	Nerbe Plus, Winsen, Germany
Masterclear® Real-time PCR film	Eppendorf, Hamburg, Germany
Microtome blades	Feather, Osaka, Japan
Nitex Mesh (70 and 100 µm)	Klein & Wieler oHG, Königswinter, Germany
Pasteur pipettes (3 ml)	Corning
Pipette tips (10, 100, 200, and 1000 µl)	Starlab, Hamburg, Germany
Reaction tubes (15 and 50 ml)	Greiner Bio-One, Kremsmünster, Austria
Safe seal reaction tubes (0.2 ml, 0.5 ml, 1.5 ml, and 2.0 ml)	Sarstedt, Nürmbrecht, Germany
Slides for IHC	Marienfeld
Tissue embedding cassettes	Marienfeld
96-well plate for Fluorescence (NuncPlate)	Thermo Fisher Scientific
384-well plate for Luminescence (ProxiPlate)	PerkinElmer, Waltham, USA

384-well qPCR plate	Applied Biosystems, Waltham, USA

2.1.3 Chemicals and reagents

Table 3: Chemicals and reagents

Chemicals / reagents	Company
Ammonium hydroxide solution 25 %	Honeywell, Selze, Germany
Ammonium Iron (III) sulfate-Dodecahydrate	Merck, Darmstadt, Germany
Antibody diluent	Dako, Hamburg, Germany
Antigen retrieval buffer	Abcam, Cambridge, UK
Dimethyl sulfoxide (DMSO)	Thermo Fisher Scientific
Dulbecco's Phosphate-buffered Saline (DPBS)	Gibco, Darmstadt, Germany
EthylenDiaminTetraAcetic Acid (EDTA)	AppliChem, Darmstadt, Germany
Eosin G	Carl Roth, Karlsruhe, Germany
Ethanol (98 %, 80 %, and 70 %)	Lohmann Laborservice GmbH, Marxen, Germany
Fetal Calf Serum (FCS)	Merck
Formaldehyde 10 %	Otto Fischar GmbH, Saarbrücken, Germany
Goat Serum	Thermo Fisher Scientific
Goldchloride	Carl Roth
Hydrogen peroxide 30 %	Carl Roth

Isopropanol	VWR International, Darmstadt, Germany
Meyer's Hematoxylin	AppliChem, Darmstadt, Germany
Murine Interleukin-3 (IL-3)	Thermo Fisher Scientific
Nuclear fast red-aluminum sulfate solution	Carl Roth
Oxalic acid	Honeywell
Paraformaldehyde (PFA) 4 %	Morphisto, Offenbach am Main, Germany
Penicillin/Streptomycin	Gibco
Potassiumhydroxide	Carl Roth
Potassiumpermanganate	Merck
ROTI® Histokitt	Carl Roth
Roswell Park Memorial Institute Medium (RPMI) 1640 Medium + GlutaMax Supple-ment	Gibco
Silvernitrate	Carl Roth
Sodium-thiosulfate-5-hydrate	VWR
Sulfuric acid 96 %	Carl Roth
SYBR Green	Thermo Fisher Scientific
Tris-HCl-buffer	AppliChem
Triton X	Thermo Fisher Scientific
Trypan blue	Gibco
Water, molecular grade	AppliChem

Xylene	Carl Roth

2.1.4 Solutions and buffers

Table 4: Solutions and buffers

Solutions / buffers	Content
Acidic potassium permanganate	Distilled water 25 % (v/v) potassium permanganate 2 % 5 % (v/v) sulfuric acid 3 %
Ammonium Iron (III) sulfate-Dodecahydrate	Distilled water 2.5 % (w/v) ammonium Iron (III) sulfate-Dodecahydrate
Blocking solution (endogenous peroxidase)	Tap water 3 % (v/v) hydrogen peroxide
Blocking solution (nonspecific binding)	TBS buffer 10 % (v/v) Goat Serum
Cell culture medium	RPMI 1640 Medium + GlutaMax 10 % (v/v) FCS 1 % (v/v) Penicillin / Streptomycin
Cell culture freezing medium	RPMI 1640 Medium + GlutaMax 20 % (v/v) FCS
Decalcification solution (pH 7.4)	Distilled water 10 % (v/v) EDTA

Goldchloride	Distilled water 0.15 % (w/v) goldchloride
Oxalic acid	Distilled water 1 % (w/v) oxalic acid
Potassiumpermanganate	Distilled water 2 % (w/v) potassiumpermanganate
Potassiumhydroxide	Distilled water 3 % (w/v) potassiumhydroxide
Silvernitrate	Distilled water 10 % (w/v) silvernitrate
Silver solution	Distilled water 10 % (v/v) silver nitrate solution 10 % 10 % (v/v) potassiumhydroxide 3 % Ammonium hydroxide solution 25 %
Sodium-thiosulfate	Distilled water 2.5 % (w/v) sodium-thiosulfate-5-hydrate
Sulfuric acid	Distilled water 3 % (v/v) sulfuric acid 96 %
Tris-Buffered Saline (TBS) buffer (wash buffer)	50 mM Tris-HCl, pH 7.5 150 mM NaCl

Wash-perm buffer	TBS buffer 0.2 % (v/v) Triton X

2.1.5 Kits and assays

Table 5: Kits and assays

Kits/assays	Company
Caspase-Glo® 1 Inflammasome Assay	Promega
Cell Meter™ Fluorimetric Intracellular Total ROS Activity Assay Kit Deep Red Fluorescence	AAT Bioquest, California, USA
EnVision FLEX DAB+ Substrate Chromogen System	Dako
Maxwell® RSC simply RNA cells and Tissue Kit	Promega
Scientific Revert Aid First Standard cDNA Synthesis Kit	Thermo Fisher Scientific

2.1.6 Antibodies

Table 6: Antibodies for IHC

Antigen	Host	Conjugate	Dilution	Company
Anti-Chicken IgY	Goat	Horseradish Peroxidase (HRP)	1:500	Abcam
Anti-Rabbit IgG	Goat	HRP	1:100	Abcam

Cluster of Differentiation (CD) 11b	Rabbit	-	1:100	Novus Biologicals, Centennial, USA
Glial Fibrillary Acidic Protein (GFAP)	Chicken	-	1:500	Biolegend, California USA
Nestin	Rabbit	-	1:100	Thermo Fisher Scietific
Tyrosine Hydroxylase (TH)	Rabbit	-	1:100	Merck

2.1.7 Primers

All oligonucleotides were synthetized by Thermo Fisher Scientific and reconstituted in molecular grade water at a concentration of 100 µM.

Table 7: Primers for RT-qPCR

Oligoname	Nucleotide sequence 5'-3'
Adrb-3 Forward	AAACTGGTTGCGAACTGTGG
Adrb-3 Reverse	TAACGCAAAGGGTTGGTGAC
COL1A1 Forward	GACAAGGGTGAGACAGGCGA
COL1A1 Reverse	GGAGACCGTTGAGTCCGCT
GAPDH Forward	CCTGCGACTTCCAACAGCAAC
GAPDH Reverse	GGATAGGGCCTCTCTTGCTC

2.1.8 Software

Table 8: Software

Software	Company
BioRender	BioRender, Toronto, Canada
CellSens Entry	Olympus
Fiji Is Just ImageJ (FIJI)	Public Domain
GraphPad Prism 9	GraphPad, La Jolla, USA
Instinct Software	Promega
Maxwell®	Promega
Microsoft Office 2022	Microsoft, Redmond, USA
NanoDrop®	Thermo Fisher Scientific
National Center for Biotechnology Information (NCBI) Primer-BLAST	NCBI, Bethesda, USA
PyRAT	Scionics Computer Innovation GmbH, Dresden, Germany
Realplex	Eppendorf
SoftMax Pro 6.3	Molecular Devices, LL, San José, USA
Zotero	Free and open-source software

2.1.9 Cell lines

The murine 32D MPL-HA cell lineages were a kind gift from Prof. Steffen Koschmieder (Aachen). All cell lineages were cultured in RPMI 1640 medium supplemented with 10 % FCS and 1 % penicillin/streptomycin. 32D MPL-HA empty vector (EV) and 32D MPL-HA

cells were cultivated in medium supplemented with 5 ng/ml murine IL-3 (IL-3 dependent growth). Cells were incubated at 37 °C with 5 % CO_2 in a cell culture incubator.

Table 9: Cell lineages

Cell lineage	Growth
32D MPL-HA *CALR-del52*	IL-3 independent
32D MPL-HA *CALR-ins5*	IL-3 independent
32D MPL-HA *JAK2V617F*	IL-3 independent
32D MPL-HA EV	IL-3 dependent
32D MPL-HA	IL-3-dependent

2.2 Mice

Mice were housed under specific pathogen-free (SPF) conditions at the House of Experimental Therapies (HET), University of Bonn. Mice were maintained in individually ventilated cages (IVC) under conventional laboratory conditions (12 h / 12 h light/dark cycle, 22 °C), with *ad libitum* access to food and water. Mice were genotyped using ear tag Deoxyribonucleic Acid (DNA) for Polymerase Chain Reaction (PCR) analysis. All animal experiments were performed with age- and sex-matched mice using male or female wildtype (C57BL/6J) or transgenic mice. Mice were sacrificed by cervical dislocation. All animal experiments were performed in accordance with the German Animal Welfare Act and approved by the government of North Rhine-Westphalia (TVA 81-02.04.2017.A488).

2.2.1 Mouse strains

Jean-Luc Villeval provided *Vav-Cre;Jak2*$^{V617F/+}$ (*Jak2*^{VF}) mice, as described in the study by Hasan et al. (Hasan et al., 2013). *Vav-Cre;Jak2*$^{V617F/+}$*;Nlrp3*$^{-/-}$ mice were generated by interbreeding of *Jak2*^{VF} mice with*Nlrp3*$^{-/-}$ mice (Millennium Pharmaceuticals). C57BL/6J mice were used as wildtype (WT) controls.

Table 10: Mouse strains

Mouse line	Genetic background	Reference	Supplier
Wildtype	C57BL/6J		Jackson Laboratories
Vav-Cre;Jak2$^{V617F/+}$	C57BL/6J	Hasan et al. Blood, 2013	Jean-Luc Villeval
Nlrp3$^{-/-}$	C57BL/6J		Millennium Pharmaceuticals
Vav-Cre;Jak2$^{V617F/+}$*;Nlrp3*$^{-/-}$	C57BL/6J		Generated by interbreeding

2.3 Methods

2.3.1 Histology

2.3.1.1 Preparation of histological slides

Femurs and spleens were removed and cleaned from surrounding tissue. Organs were fixed in 4 % PFA at 4 °C overnight. After fixation, femurs were decalcified in a decalcification solution (Table 4) at 56 °C in a water bath for two days. At the department for Dermatopathology, University Bonn, tissue samples were paraffin embedded. Paraffined samples were cut 4 µm thick using the microtome, transferred to specimen slides and dried at 36 °C overnight. Before staining, samples were dehydrated in xylene followed by 98 %, 80 % and 70 % ethanol.

2.3.1.2 Immunohistochemistry

After deparaffination and rehydration antigen retrieval was performed with Antigen Retrieval buffer for 10 minutes in a steam cooker and samples were cooled for 10 minutes. Blocking was performed with endogenous peroxidase using 3 % hydrogen peroxide (for 5 minutes at room temperature (RT), and sequentially 10 % goat serum (for one hour at RT). The primary antibodies (CD11b, Nestin, TH and GFAP) incubated overnight at 4 °C

in the dark. The secondary HRP-conjugated antibody incubated for one hour at RT protected from light. For visualization EnVision FLEX DAB+ Substrate Chromogen System was added (incubation time of 7-10 minutes at RT, protected from light). Samples were counterstained in Mayer's Hematoxylin solution, rehydrated in 70 %, 90 % and 98 % ethanol, cleared with xylene and were mounted. Positive cells appeared brown whilst negative cells were purple and spleen sections of WT mice stained for CD11b served as positive controls. Positive cell counts for nestin, GFAP, and TH were determined through manual counting. Multiple high-power fields (HPFs) per mouse were analyzed in a blinded manner, and the mean count per animal was calculated. Nestin$^+$ cells were described using the following score.

Table 11: Score for Nestin staining

Term	Description
Niches	Clusters of up to three nestin$^+$ cells located in the bone marrow
Perivascular niche	Nestin$^+$ perivascular cells
Endostal niche	Nestin$^+$ periosteal cells

2.3.1.3 Gordon & Sweet's staining

After dehydration femur and spleen tissue sections were stained with acidic potassium permanganate for 3 minutes and then washed with tap water until clean. The slides were bleached with oxalic acid 1 % for 1 minute and stained with ammonium iron (III) sulfate 2.5 % for 15 minutes. Then the application of the silver solution followed. Samples were put into the ammoniacal silver solution for 10 seconds. Washing in formalin 10 % for 20 seconds followed. Samples were toned with gold chloride 0.15 % for 1 minute and fixed with sodium-thiosulfate 2.5 % for 3 minutes. After washing the slides, they were counterstained with nuclear fast red-aluminum sulfate solution for 13 minutes. Finally, samples were rehydrated in 70 %, 90 % and 98 % ethanol, cleared with xylene and were mounted.

Reticular fibers appeared black whilst cells were stained purple. Myelofibrosis (MF) and splenic fibrosis were assessed using the following grading systems.

Table 12: WHO 2008 grading system for myelofibrosis (Kvasnicka et al., 2016)

Grade	Description
MF-0	Scattered linear reticulin with no intersections (crossovers) corresponding to normal bone marrow
MF-1	Loose network of reticulin with many intersections, especially in perivascular areas
MF-2	Diffuse and dense increase in reticulin with extensive intersection, occasionally with focal bundles of thick fibers mostly consistent with collagen and/or focal osteosclerosis
MF-3	Diffuse and dense increase in reticulin with extensive intersections and coarse bindles of thick fibers mostly consistent with collagen, usually associated with osteosclerosis

Table 13: Grading of splenic fibrosis, score recommended by the National Toxicology Program (Hobbie et al., 2014)

Grade	Description
Grade 0	Fine fibers around the splenic vessels and red pulp sinusoids, corresponding to normal parenchymal structure
Grade 1	Subcapsular fibrosis

Grade 2	Parenchymal fibrosis extending into the marginal zone
Grade 3	Parenchymal fibrosis infiltrating the white pulp

2.3.1.4 Hematoxylin and Eosin (H&E) staining

Femur and spleen samples were shortly put in Meyer's Hematoxylin (approx. 15 seconds). After washing in tap water and distilled water for 2 minutes slides were put in Eosin G solution for 3 minutes. After washing in tap water rehydration and mounting followed. The quantification of megakaryocytes per HPF (50X) involved manual counting, while the size and morphology of megakaryocytes was measured using FIJI software. Megakaryocytes in BM and spleen were analyzed in a blinded fashion. Additionally, osteosclerosis was assessed using the following grading system.

Table 14: Grading of Osteosclerosis (Kvasnicka et al., 2016)

Grade	Description
Grade 0	Regular bone trabeculae (distinct paratrabecular borders)
Grade 1	Focal budding, hooks, spikes or paratrabecular apoosition of new bone
Grade 2	Diffuse paratrabecular new bone formation with thickening of trabeculae, occasionally with focal interconections
Grade 3	Extensive interconnecting meshwork of new bone with overall effacement of marrow spaces

2.3.1.5 Image acquisition and analysis

Samples were examined using the Olympus BX51 microscope and images of the samples were acquired using CellSens software. Image analysis involved manual counting, FIJI software and scores for grading (tables 11-15), which were analyzed in a blinded fashion.

2.3.2 Real-time quantitative polymerase chain reaction (RT-qPCR)

2.3.2.1 Ribonucleic acid (RNA) isolation and complementary DNA (cDNA) synthesis

One femur and tibia each were removed, cleaned from surrounding tissue and the epiphysis were cut. Bone marrow cells were flushed using a centrifuge. After washing, bone marrow cells were filtered through a 70 µm nylon mesh. Total RNA was isolated using the Maxwell® RSC 48 using the Maxwell® RSC simplyRNA Tissue kit. RNA concentration was determined with a spectrophotometer using 1 µl of sample for the measurement. RNA samples were stored at -80 °C. For the reverse transcription, 5 µg of RNA per sample were used in a reaction volume of 20 µl containing molecular grade water, random primers, buffer, riboblock inhibitor, dNTPs, and reverse transcriptase according to the manufacturer's instructions (Scientific Revert Aid First Standard cDNA Synthesis Kit). Subsequently, the cDNA synthesis was carried out in the following steps: primer annealing for 5 minutes at RT, DNA polymerization for 60 minutes at 42 °C and enzyme deactivation for 5 minutes at 70 °C. cDNA was then either immediately used for qPCR or stored at -20 °C.

2.3.2.2 RT-qPCR

SYBR-green based RT-qPCR was used to determine relative gene expression. qPCR reactions were done in 96 well plates covered by an adhesive film. Primers were diluted 10x and reactions were prepared as follows: 5 µl of cDNA and 15 µl of mastermix containing SYBR Green, forward and reverse primer and sterile water. All the reactions were performed in technical triplicates, from which one was used as negative control containing no cDNA. Glyceraldehyde 3-phosphate dehydrogenase (GAPDH) was used as housekeeping gene and the genes of interest were *Adrb3* and *COL1A1* (primer sequences are listed in Table 7). RT-qPCR was carried out with the Mastercycler realplex^2. The amplification program used always included a melting curve analysis at the end to ascertain that the amplification was target specific. Primer sequences for *Adrb3*, *COLA1A1* and *GAPDH* were designed using NCBI Primer-BLAST and tested for specificity and amplification performance. For each primer pair, a standard curve was generated using a serial dilution of

cDNA. All primers showed high efficiency, with slope values ranging between -3.1 and -3.6 and correlation coefficients (R^2) close to 0.99, corresponding to amplification efficiencies within the accepted range of 90-110%. Specificity of each primer pair was further confirmed by melting curve analysis, showing single, distinct peaks. These results confirm the validity of the primers and justify the use of the delta-delta Cycle threshold (ΔΔCt) method for relative gene expression analysis. Based on the validated ΔΔCt approach, relative gene expression levels were quantified and normalized to the control group (C57/BL6 mice).

2.3.3 In vitro cell culture

2.3.3.1 Cultivation and counting

The general cell culture conditions were 37 °C with 5 % Carbon dioxide (CO_2) in a humidified atmosphere. 32D cells were cultured in 25 cm^2 culture flasks containing 5 ml cell culture medium for one day followed by cultivation in 15 ml medium in 75 cm^2 culture flaks. Cells were passaged every second to third day at a ratio of 1:3 to 1:5 to maintain a density of 0.5 – 1.0×10^6 cells / 1 ml. Media and PBS were warmed to 37 °C before usage. The cells were handled under a sterile laminar flow workbench and morphologically evaluated using a phase-contrast light microscope. Living cells were counted manually in a standard Neubauer hemocytometer, excluding dead cells by trypan blue staining.

2.3.3.2 Freezing and thawing

Cells were frozen at a density of 2×10^7 / 1 ml of cell culture freezing medium. The cell suspension was transferred to cryo-vials and frozen in isopropanol freezing containers at -80 °C for 24 hours and transferred to -150 °C for permanent storage. Cells were thawed at 37 °C in a water bath until almost all ice was melted. Cell suspension was immediately transferred to 12 ml of pre-warmed medium and pelleted at 500 g for 3 minutes. Cells were washed twice with PBS to remove DMSO completely. Cells were then resuspended in fresh medium and cultured.

2.3.3.3 Caspase-Glo Inflammasome Assay

3.0×10^4 cells / well were seeded into a 96-well plate in 50 µl RPMI medium. Cells were cultured with or without murine IL-3 as depicted in Table 9 and HA-EV cells served as wildtype controls. Technical triplicates of cells and their corresponding supernatant from

each cell lineage were used. Cells were spinned at 500 g for 2 minutes at RT. To a 384-well plate 8 µl of supernatant and 8 µl of resuspended cells were transferred. 8 µl of Caspase-GLO 1 reagent was added to all samples including blank samples containing medium only (background luminescence). Caspase-GLO 1 reagent contained a luminogenic caspase-1 substrate (Z-WEHD-aminoluciferin) and thermostable, recombinant luciferase. Plate was covered with a sealer and mixed on a plate shaker for 30 seconds. Subsequently, luminescence was measured every 30 minutes at seven times. Results were recorded using a GloMax Multi+ Detection System.

2.3.3.4 Intracellular ROS production assay

1.0×10^5 cells / well were seeded into a 96-well plate in 50 µl RPMI medium. Cells were cultured with or without murine IL-3 as depicted in Table 9 and HA-EV cells served as wildtype controls. 50 µl of 0.3 % Hydrogen Peroxide (H_2O_2) was added to positive controls to elicit intracellular ROS production. Technical triplicates of cells from each cell lineage were used. Cells were washed with PBS and resuspended in 100 µl of 100X ROS Brite™ 670 nonfluorescent working solution. After an incubation time of 30 minutes at 37 °C and 5 % CO_2, cells were transferred to a flat bottom white 96-well plate, and fluorescence was measured at Ex/Em = 650/675 nm by a SpectraMax i3 system.

2.3.4 Statistical analysis

Statistical analyses and graphics were carried out with Graph-Pad Prism 9 software. Data sets were compared using non-parametric tests indicated in the description of graphs. The *p*-value was calculated to indicate statistical significance and is denoted with asterisks (*$^*P<0.05$, $^{**}P<0.01$, $^{***}P<0.001$, $^{****}P<0.0001$*).

3 Results

3.1 Spontaneous inflammasome activation in MPN

To test for inflammasome activation in MPN, murine cell lines stably transduced with the known driver mutations in BCR-ABL negative MPN (*JAK2V617F*, *CALR-del52* and *CALR-ins*5) and controls with an empty vector (HA-EV cells) were investigated. NLRP3 mediates Caspase-1 activation (Kelley et al., 2019), which makes Caspase-1 a reliable marker of inflammasome activation. To assess Caspase-1 activation, cells and their supernatant were treated with Caspase-Glo 1 Reagent, which induces cleavage of luminogenic caspase-1 substrate and generation of a luminescent signal by luciferase proportional to caspase-1 activity. Caspase-1 activity of cells was significantly higher in *JAK2V617F, CALR-del52* and *CALR-ins*5 cell lineages compared to WT controls. Measurement of supernatants of *JAK2V617F, CALR-del52* and *CALR-ins5* cells showed a comparable pattern (Figures 4A and 4B).

ROS are DAMPS that are secreted after cell activation or damage and can lead to the transcriptional upregulation of NLRP3 ("priming"), which is required for inflammasome activation (Bauernfeind et al., 2011; Ratajczak et al., 2020). ROS production was measured by a fluorescent signal of cells after incubation with a nonfluorescent (ROS brite working solution), which produces bright fluorescence upon reaction with hydroxyl radicals. Evaluation of intracellular ROS production revealed significantly higher ROS levels in cells expressing *JAK2V617F, CALR-del52* or *CALR-ins5* mutation compared to the control group (Figure 4C).

These findings indicate *in vitro* spontaneous inflammasome activation in MPN.

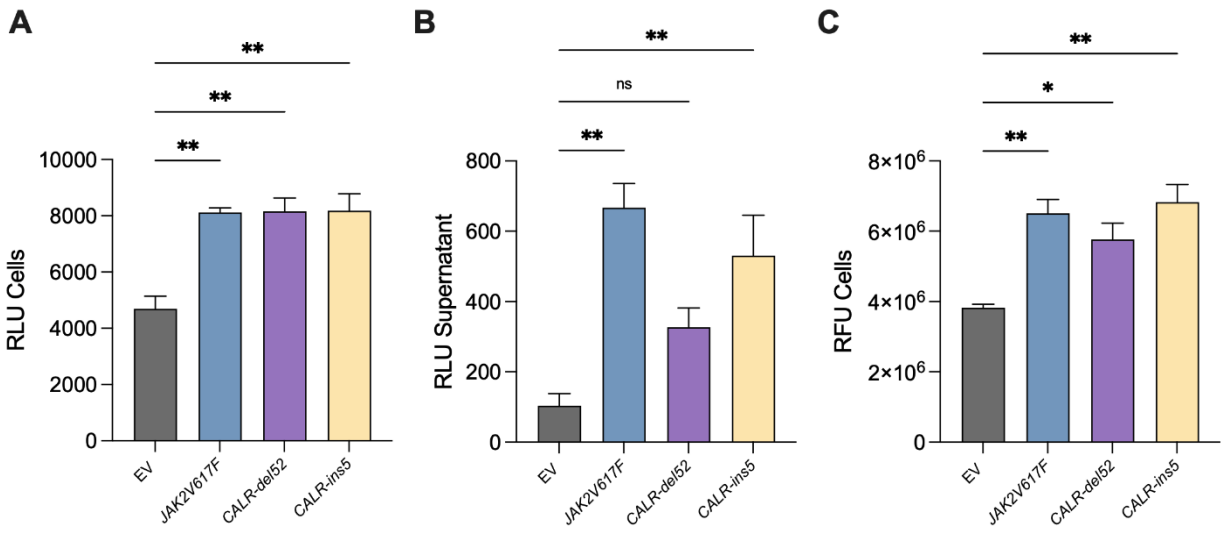

Figure 4: Inflammasome activation in MPN.

(**A, B**) Luminescence of 32D cells and their supernatant (HA-EV, *JAK2V617F, CALRdel52, CALRins5)* after 180 minutes of incubation with Caspase-Glo 1 Reagent for analysis of Caspase 1 activity. Technical triplicates of cells and supernatant of each cell lineage were used. The luminescent signal is proportional to caspase-1 activity. Luminescence (RLU, Relative Luminescence Unit) is shown.
(**C**) Fluorescence of 32D cells (HA-EV, *JAK2V617F, CALRdel52, CALRins5*) after 30 minutes of incubation with ROS Brite 679 working solution for quantification of ROS production. Technical triplicates of cells of each cell lineage were used. The level of ROS production was quantified by the fluorescent intensity of the ROS Brite 670 dye. Fluorescence (RFU, Relative Fluorescence Unit) is shown.
Columns represent mean + Statistical Error of the Mean (SEM). Statistically significant differences were determined by one-way ANOVA followed by Dunnett's multiple comparison test for multiple comparisons. **P<0.05, **P<0.01.*

3.2 *Nlrp3* deficiency in *Jak2^{VF}* mice reduces fibrosis in BM and spleen and regulates excess megakaryopoiesis

Excerpts of the following results were published by Koerber et al. (2024). These include the scoring for BM fibrosis and splenic fibrosis, as well as the analysis of the number of megakaryocytes and the representative images for fibrosis and megakaryocytes (Koerber et al., 2024). To enhance the understanding of the subsequent context, these findings are presented in the following section.

To examine, whether NLRP3 contributes to fibrotic and megakaryocytic changes, *Nlrp3* knock-out mice harboring the *Jak2^{VF}* mutation were generated. BM and spleen sections of *Jak2^{VF}*, *Jak2^{VF};Nlrp3$^{-/-}$* and WT mice were stained with Gordon & Sweet's silver staining

to assess fibrosis development in the pre- and absence of NLRP3. Grading of fibrosis revealed a significant reduction of fibrosis in BM and spleen of *Jak2*^{VF}*;Nlrp3*$^{-/-}$ mice compared to the *Jak2*^{VF} group (Figures 5B and 5C). Additionally, the transcriptional expression level of *COL1A1* (Collagen, type I, alpha 1) was assessed. *COL1A1* represents a fibrosis-associated gene, with collagen I being a frequent protein in the ECM and serving as the unique ECM protein linked to fibrosis (Leimkühler et al., 2021). RT-qPCR was performed on whole BM cells of *Jak2*^{VF}, *Jak2*^{VF}*;Nlrp3*$^{-/-}$ and WT mice and expression level of *COL1A1* was compared among the groups. As hypothesized, the expression level of *COL1A1* was notably downregulated in *Jak2*^{VF}*;Nlrp3*$^{-/-}$ mice compared to *Jak2*^{VF} mice (Figure 5D). These findings suggest that the absence of NLRP3 in *Jak2*^{VF} mice leads to a decrease in fibrosis observed in both BM and spleen. Osteosclerosis, often associated with fibrosis, was examined in the subsequent analysis.

A

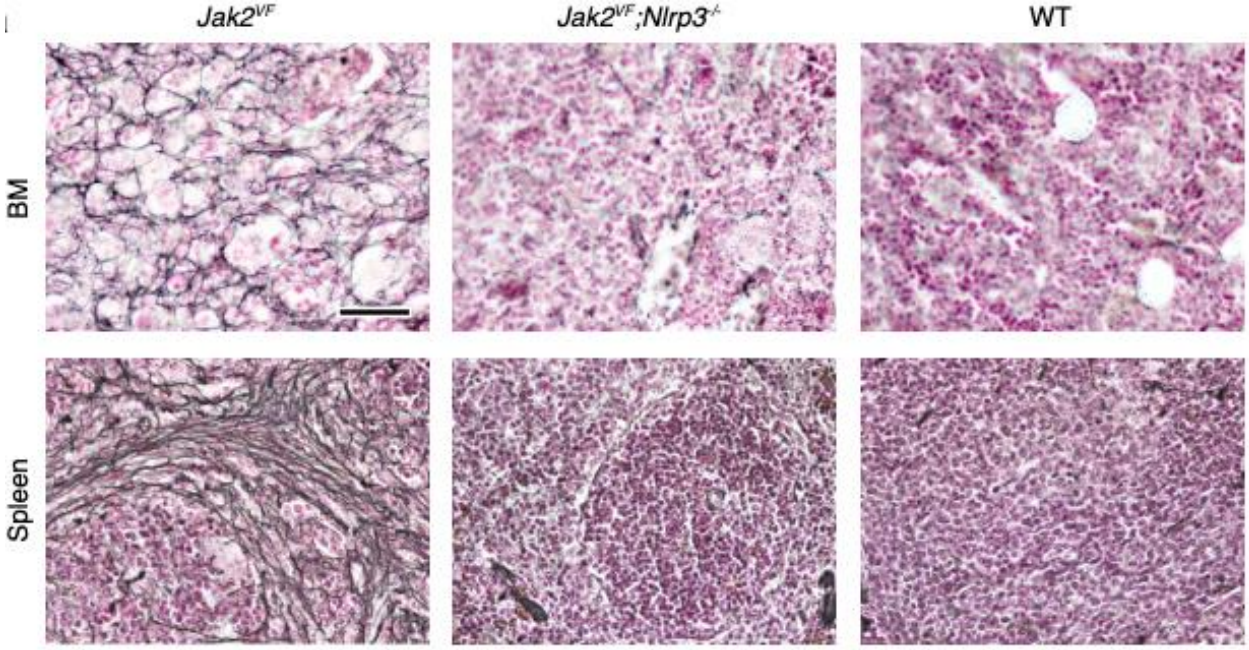

B

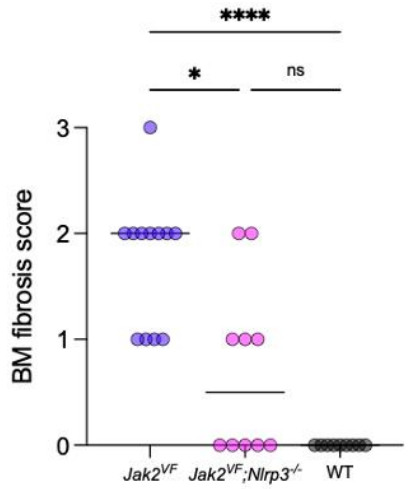

Genotype	*Jak2*^{VF}	*Jak2*^{VF}*;Nlrp3*$^{-/-}$	WT
Number of mice	12	10	9
Fibrosis score (%)			
0	0	5 (50)	9 (100)
1	4 (33,3)	3 (30)	0
2	7 (58,3)	2 (20)	0
3	1 (8,3)	0	0

C

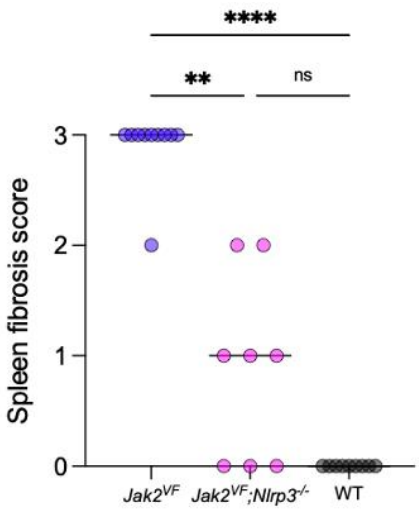

Genotype	*Jak2*^{VF}	*Jak2*^{VF}*;Nlrp3*$^{-/-}$	WT
Number of mice	10	8	9
Fibrosis score (%)			
0	0	3 (37,5)	9 (100)
1	0	3 (37,5)	0
2	1 (10)	2 (25)	0
3	9 (90)	0	0

D

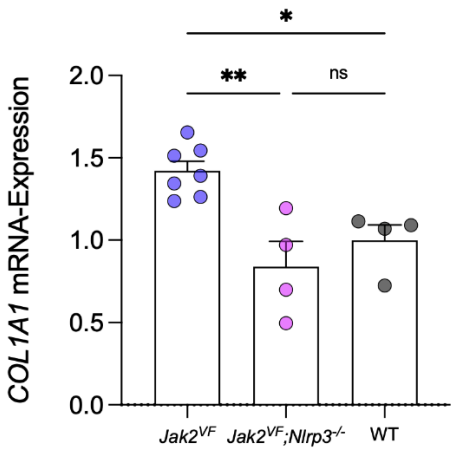

Figure 5: *Nlrp3* deficiency in *Jak2^{VF}* mice reduces fibrosis in BM and spleen.

(**A**) Representative images of silver-stained BM (femur) and spleen sections of *Jak2^{VF}*, *Jak2^{VF};Nlrp3$^{-/-}$* and WT mice at 26 weeks of age for grading of fibrosis. Scale bar equals 50 µm (Koerber et al., 2024).
(**B**) Fibrosis of BM was scored from 0 to 3 in a blinded fashion. Scores of *Jak2^{VF}* (n=12), *Jak2^{VF};Nlrp3$^{-/-}$* (n=10) and WT (n=9) mice at 26 weeks of age are shown in a Dot-Plot and a table format.
(**C**) Fibrosis of spleen was scored from 0 to 3 in a blinded fashion. Scores of *Jak2^{VF}* (n=10), *Jak2^{VF};Nlrp3$^{-/-}$* (n=8) and WT (n=9) mice at 26 weeks of age are shown in a Dot-Plot and a table format.
In scatter plots each dot represents an animal and horizontal lines the median. Statistically significant differences were determined by Kruskal-Wallis test with Dunn's multiple comparison test. **P<0.5, **P<0.01, ****P<0.0001.*
(**D**) RT-qPCR from BM (femur) cells from *Jak2^{VF}* (n=7), *Jak2^{VF};Nlrp3$^{-/-}$* (n=4) and WT (n=4) mice at 26 weeks of age for investigation of expression levels of *COL1A1*.
Data analysis was performed using delta-delta-Ct (ΔΔCt) values. Columns show mean + SEM. Statistically significant differences were determined by one-way ANOVA followed by Tukey's multiple comparison test for multiple group comparisons. **P<0.05, **P<0.01.*

In MPN, osteosclerosis is observed due to overproduction of inflammatory cytokines leading to an abnormal expansion of osteoblasts. To assess changes in its extent depending on NLRP3, osteosclerosis in the BM of *Jak2^{VF}*, *Jak2^{VF};Nlrp3$^{-/-}$* and WT mice was scored. Osteosclerosis trended to be less severe in *Jak2^{VF};Nlrp3$^{-/-}$* mice compared to *Jak2^{VF}* mice, though change did not reach a significant level (Figure 6).

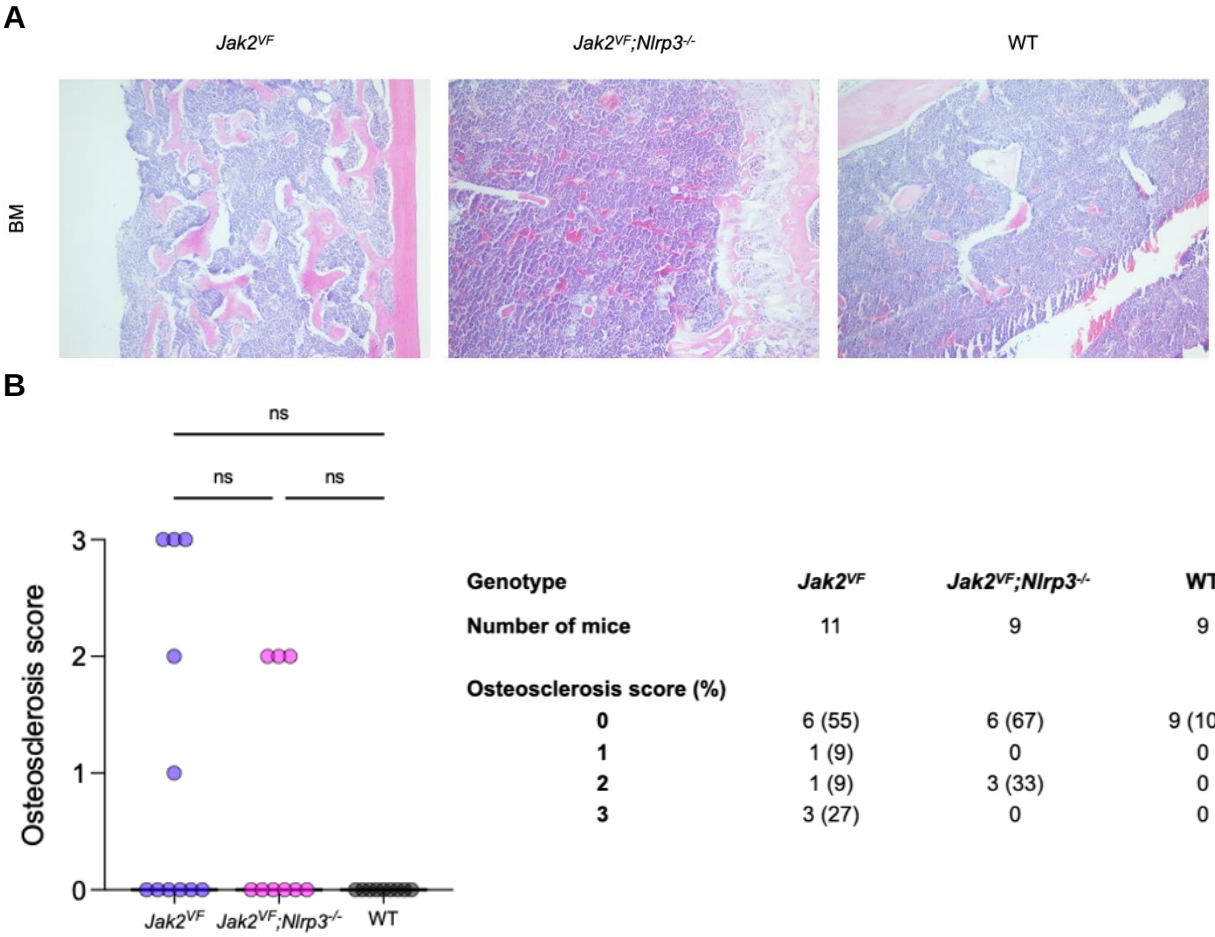

Genotype	*Jak2*^{VF}	*Jak2*^{VF}*;Nlrp3*$^{-/-}$	WT
Number of mice	11	9	9
Osteosclerosis score (%)			
0	6 (55)	6 (67)	9 (100)
1	1 (9)	0	0
2	1 (9)	3 (33)	0
3	3 (27)	0	0

Figure 6: *Nlrp3* deficiency in *Jak2*^{VF} mice ameliorates osteosclerosis in BM.

(A) Representative images of H&E-stained BM (femur) sections of *Jak2*^{VF}, *Jak2*^{VF}*;Nlrp3*$^{-/-}$ and WT mice at 26 weeks of age for grading of osteosclerosis. 10X magnification.
(B) Osteosclerosis of BM was scored from 0 to 3 in a blinded fashion. Scores of *Jak2*^{VF} (n=11),
Jak2^{VF}*;Nlrp3*$^{-/-}$ (n=9) and WT (n=9) mice at 26 weeks of age are shown in a Dot-Plot and table format.
In scatter plots each dot represents an animal and horizontal lines the median. Statistically differences were determined by Kruskal-Wallis test followed by Dunn's multiple comparison test.

Megakaryocytic hyperplasia and dysplasia of megacaryocytes are common and characteristic features in MPN (Ghosh et al., 2023). To assess impacts of the NLRP3 inflammasome in MPN megakaryopoiesis, the number of megakaryocytes in BM and spleen sections of *Jak2*^{VF}, *Jak2*^{VF}*;Nlrp3*$^{-/-}$ and WT mice was evaluated. The size of megakaryocytes in BM mice and spleen sections of *Jak2*^{VF}, *Jak2*^{VF}*;Nlrp3*$^{-/-}$ and WT mice was meas-

ured using FIJI software. BM and spleen of *Jak2*^{VF} mice lacking NLPR3 showed significantly fewer megakaryocytes than *Jak2*^{VF} with a competent inflammasome (Figure 7). A similar pattern was noted in the size of megakaryocytes. These results suggest that the NLRP3 inflammasome may play a role in megakaryopiesis in MPN as indicated by reduced numbers and sizes of megakaryocytes in BM and spleen sections of *Jak2*^{VF}*;Nlrp3*$^{-/-}$ mice compared to *Jak2*^{VF} mice. It can be concluded that *Nlrp3* deficiency results in reduction of fibrosis and normalization of megakaryopoiesis in *Jak2*^{VF} mice.

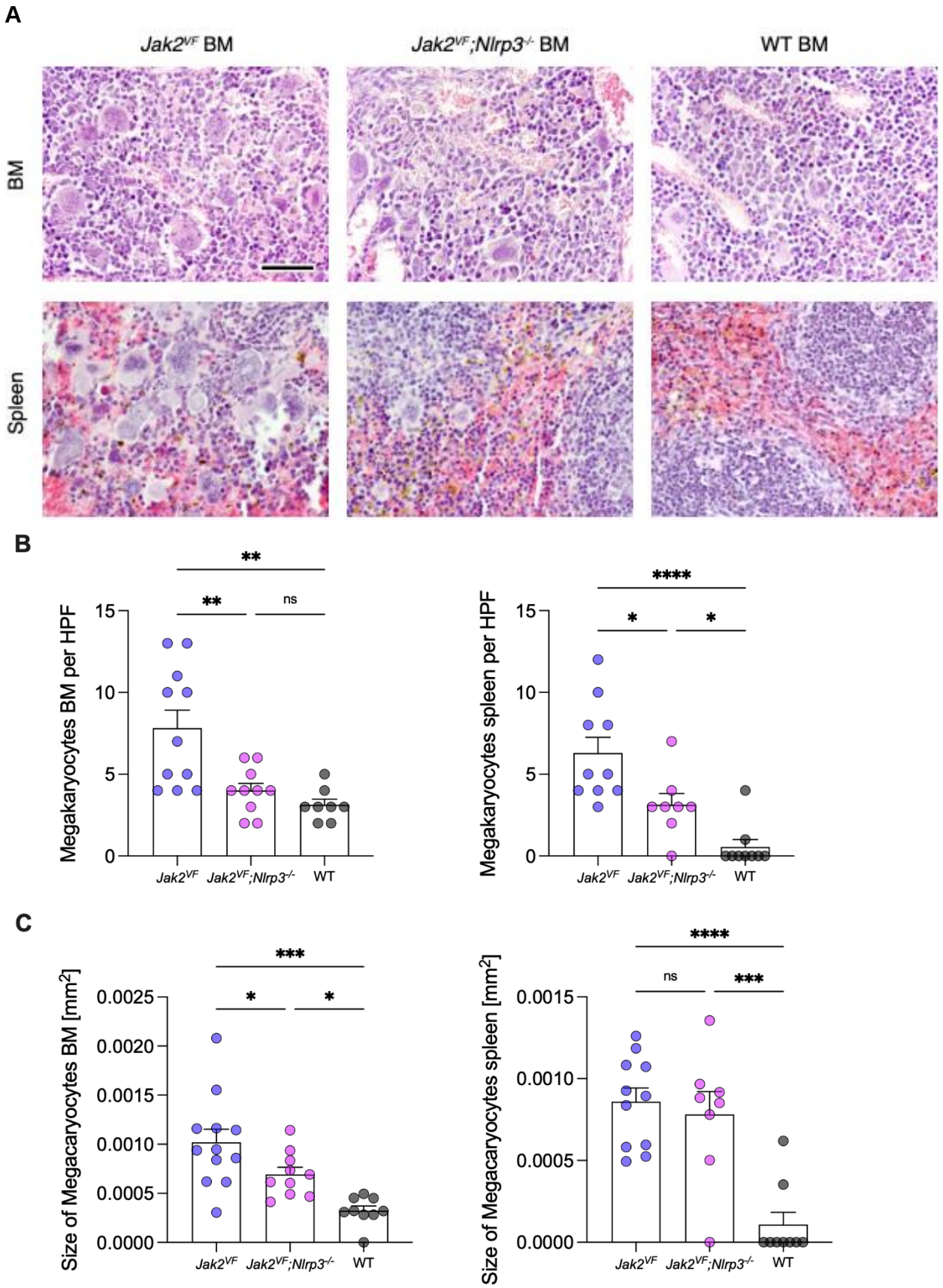

Figure 7: NLRP3 drives megakaryopoiesis in murine MPN.

(**A**) Representative images of H&E-stained BM (femur) and spleen sections of *Jak2*^{VF}, *Jak2*^{VF}*;Nlrp3*$^{-/-}$ and WT mice at 26 weeks of age illustrating the density of megakaryocytes. Scale bar equals 50 µm, (Koerber et al., 2024).
(**B**) Number of megakaryocytes in *Jak2*^{VF} (BM n=11, spleen n=10), *Jak2*^{VF}*;Nlrp3*$^{-/-}$ (BM n=10, spleen n=8) and WT (BM n=8, spleen n=9) mice 26 weeks of age (HPF, high-power field).
(**C**) Size of megakaryocytes in *Jak2*^{VF} (BM n=12, spleen n=11), *Jak2*^{VF}*;Nlrp3*$^{-/-}$ (BM n=10, spleen n=8) and WT (BM n=9, spleen n=9) mice 26 weeks of age in mm^2 (HPF, high-power field).
Megakaryocytes of several HPFs per mouse were manually counted in a blinded fashion and measured using FIJI software. The mean size of megakaryocytes for each mouse was calculated. Each dot represents a mouse. Plots show mean + SEM. Statistically significant differences were determined by one-way ANOVA followed by Holm-Šidák multiple comparison test for multiple comparisons. **P<0.05, **P<0.01, ***P<0.001, **** P<0.0001.*

3.3 *Nlrp3* deficiency in *Jak2*^{VF} mice restores nestin$^+$ MSCs and sympathetic bone marrow innervation in MPN

The key effector cytokine of the NLRP3 inflammasome IL-1β plays a central role in mediating inflammatory responses (Parciante et al., 2023). To investigate IL-1β driven neuropathy and MSC loss in MPN, BM sections of *Jak2*^{VF}, *Jak2*^{VF}*;Nlrp3*$^{-/-}$ and WT mice were analyzed.

Nestin was used as a marker for MSCs that are associated with HSC regulation (García-García et al., 2015). Positive cells were counted manually in a blinded fashion and nestin$^+$ cells were scored as depicted in Table 12. In *Jak2*^{VF} and *Jak2*^{VF}*;Nlrp3*$^{-/-}$ mice, nestin$^+$ niches were notably reduced compared to the WT group. However, differences between *Jak2*^{VF} and *Jak2*^{VF}*;Nlrp3*$^{-/-}$ were not significant. The count of nestin$^+$ perivascular niches was significantly lower in *Jak2*^{VF} mice compared to the healthy controls. In *Jak2*^{VF}*;Nlrp3*$^{-/-}$ mice, the number of nestin$^+$ perivascular niches approached normalization, showing no significant differences compared to WT controls and a marked increase compared to *Jak2*^{VF} mice (Figure 9). The number of nestin$^+$ endostal niches was highest in *Jak2*^{VF} and differences between *Jak2*^{VF} and *Jak2*^{VF}*;Nlrp3*$^{-/-}$ mice were not significant (data not shown). In total, nestin$^+$ cells were highest in WT mice, followed by *Jak2*^{VF}*;Nlrp3*$^{-/-}$ and WT mice indicating that the NLRP3 inflammasome drives MSC loss in MPN.

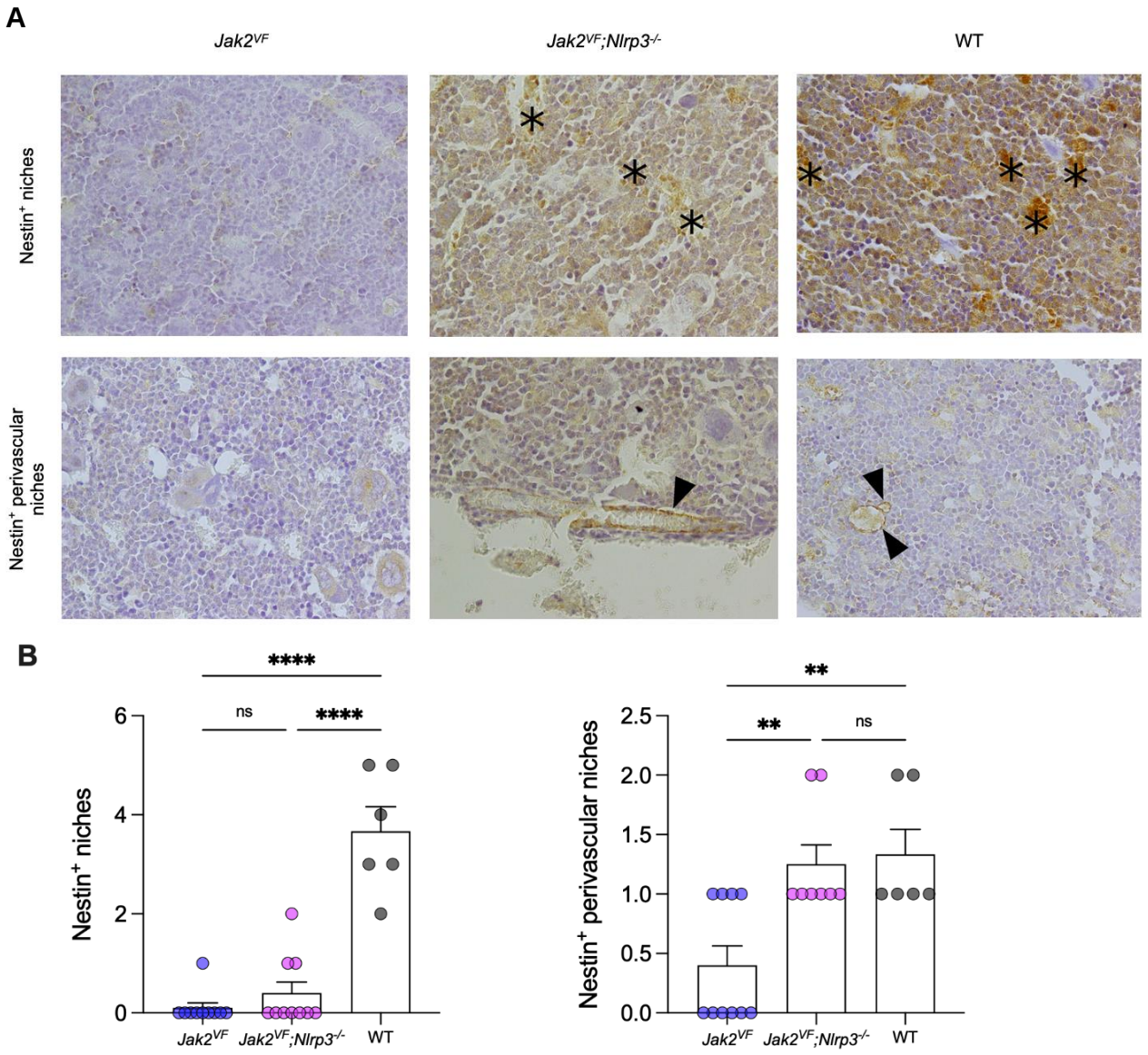

Figure 8: *Nlrp3* deficiency in *Jak2^{VF}* mice restores nestin^{+} MSCs.

(**A**) Representative images of nestin-stained BM (femur) sections of *Jak2^{VF}* (n=10), *Jak2^{VF};Nlrp3$^{-/-}$* (n=10) and WT(n=9) mice at 26 weeks of age for analysis of nestin^{+} MSCs. 50X magnification. Nestin^{+} niches are marked by asterisks and perivascular niches by arrows.
(**B**) Nestin^{+} niches and perivascular niches of BM (femur) sections of *Jak2^{VF}*, *Jak2^{VF};Nlrp3$^{-/-}$* and WT mice at 26 weeks of age were counted manually. Several HPFs per mouse were analyzed in a blinded fashion (HPF, high power field). The mean of nestin^{+} cells for each animal was calculated. Each dot represents a mouse. Plots show mean + SEM. Statistically significant differences were determined by one-way Analysis of Variance (ANOVA) followed by Holm-Šidák multiple comparison test for multiple comparisons. **P<0.05, **P<0.01, ***P<0.001, ****P<0.0001.*

Neuropathy was assessed by TH staining for sympathetic nerve fibers and GFAP staining for Schwann cells. Positive cells were counted manually in a blinded fashion. Sympathetic nerve fibers and Schwann cells were notably reduced in the BM of *Jak2*^{VF} mice compared to the WT group. The neuroglial damage observed in *Jak2*^{VF} mice was mitigated in *Jak2*^{VF}*;Nlrp3*$^{-/-}$ mice, as evidenced by an increased number of TH^{+} and GFAP^{+} cells compared to *Jak2*^{VF} mice (Figures 10B and 10C).

Additionally, the transcriptional expression level of *Adrb3 (*β-3-adrenergic receptor) was assessed. The β-3-adrenergic receptor encoded by *Adrb3* is expressed in nestin^{+} MSC and is involved in HSC trafficking (Méndez-Ferrer et al., 2008). Loss of *Adrb3* leads to accelerated MPN progression (Arranz et al., 2014). RT-qPCR was performed on whole BM cells of *Jak2*^{VF}, *Jak2*^{VF}*;Nlrp3*$^{-/-}$ and WT mice and expression level of *Adrb3* was compared among the groups. In *Jak2*^{VF}*;Nlrp3*$^{-/-}$ mice the expression of *Adrb3* was upregulated compared to the *Jak2*^{VF} group (Figure 10D).

This analysis reveals that *Nlrp3* deficiency in *Jak2*^{VF} mice mitigates neuroglial damage reflected by normalization in number of sympathetic nerve fibers, ensheathing Schwann cells and β-3-adrenergic receptor expression.

Taken together, these results indicate that the NLRP3 inflammasome aggravates neural damage, thereby compromising MSC survival in MPN.

A

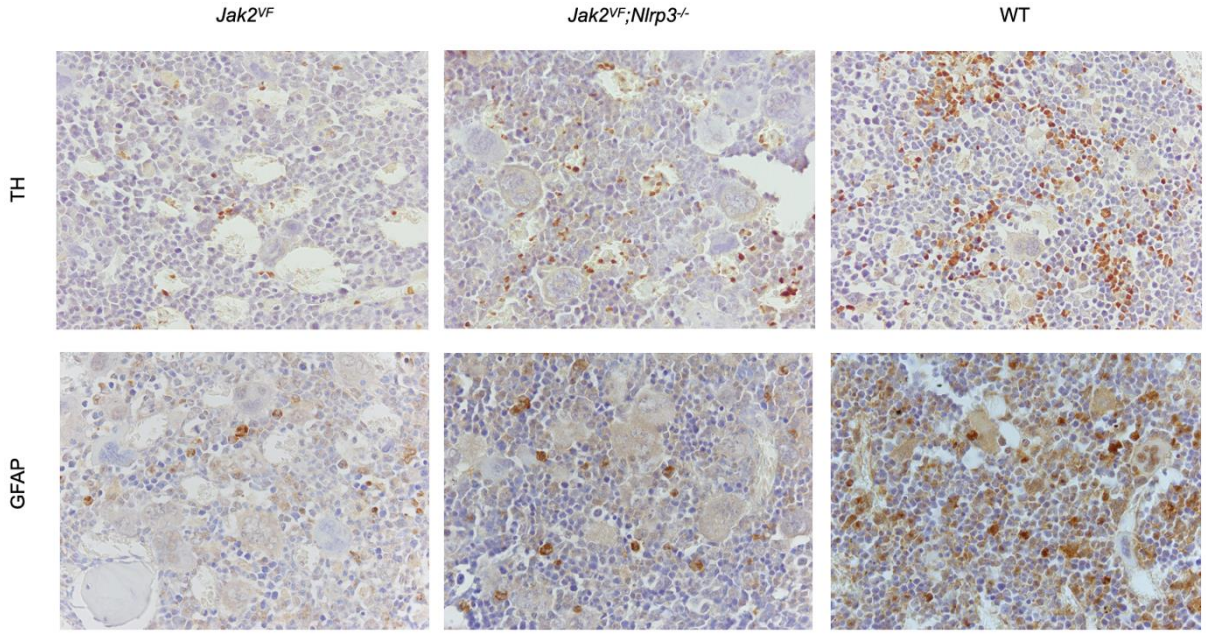

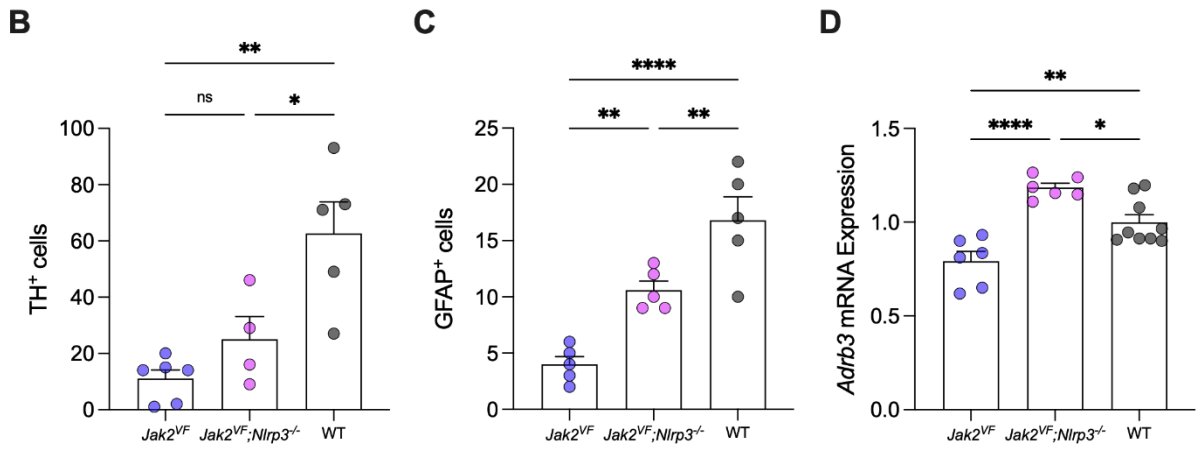

Figure 9: *Nlrp3* deficiency in *Jak2*^{VF} mice restores sympathetic BM innervation.

(**A**) Representative images of TH- and GFAP-stained BM (femur) sections of *Jak2*^{VF}, *Jak2*^{VF}*;Nlrp3*$^{-/-}$ and WT mice at 26 weeks of age for analysis of TH-positive cells and GFAP-positive Schwann cells. 50X magnification.
(**B**) TH-positive cells of BM (femur) sections of *Jak2*^{VF} (n=6), *Jak2*^{VF}*;Nlrp3*$^{-/-}$ (n=4) and WT (n=5) mice at 26 weeks of age were counted manually.
(**C**) GFAP-positive cells of BM (femur) sections of *Jak2*^{VF} (n=6), *Jak2*^{VF}*;Nlrp3*$^{-/-}$ (n=5) and WT (n=5) mice at 26 weeks of age were counted manually.
Several HPFs per mouse were analyzed in a blinded fashion (HPF, high power field). The mean of TH- and GFAP-positive cells for each animal was calculated. Each dot represents a mouse. Plots show mean + SEM. Statistically significant differences were determined by one-way ANOVA with Holm-Šidák multiple comparison test. *P<0.05, **$P<0.01$ ****$P<0.0001$.
(**D**) RT-qPCR from BM (femur) cells from *Jak2*^{VF} (n=6), *Jak2*^{VF}*;Nlrp3*$^{-/-}$ (n=6) and WT (n=9) mice at 26 weeks of age for investigation of expression levels of *Adrb3*.
Data analysis was performed using delta-delta-Ct (ΔΔCt) values. Columns show mean + SEM. Statistically significant differences were determined by one-way ANOVA followed by Tukey's multiple comparison test for multiple comparisons. *$P<0.05$, **$P<0.01$, ****$P<0.0001$.

4 Discussion

This thesis reveals how the NLRP3 inflammasome contributes to the development of MPN by focusing on fibrotic changes in the BM, neural damage of the hematopoietic stem cell niche and MSC survival as a regulator for HSCs. Notably, spontaneous inflammasome activation in MPN cell lines was detected in vitro. Fibrosis in the BM and spleen was reduced and megakaryopoiesis normalized in *Jak2*^{VF} mice lacking *Nlrp3*. BM neuropathy, a characteristic of MPN, was ameliorated and MSCs restored in *Jak2*^{VF}*;Nlrp3*$^{-/-}$ mice.

4.1 Spontaneous inflammasome activation in MPN

Chronic sterile inflammation is a defining characteristic of MPN (Koschmieder et al., 2016) driven by various factors including heightened production of pro-inflammatory cytokines, oxidative stress, and alterations in the BM microenvironment (Bjørn and Hasselbalch, 2015). Inflammasomes, particularly the NLRP3 inflammasome, are of specific interest as they play a central role in exacerbating inflammation. The NLRP3 inflammasome is responsible for production of the cytokines IL-1β and IL-18, which are implicated in driving MPN progression (Parciante et al., 2023). To gain a better understanding of the role of inflammation in MPN, inflammasome activity was measured in a murine cell line model expressing MPN driver mutations. Caspase-1, directly linked to NLRP3 and serving as its main effector caspase during inflammasome activation, was used as a marker of inflammasome activity. Caspase-1 activity was measured via luminescence in *JAK2V617F, CALR-del52* and *CALR-ins5* mutated cells. Results showed that Caspase-1 activity was markedly higher in cell lines expressing a driver mutation for BCR-ABL negative MPN than in the WT control. This indicates that spontaneous inflammasome activity is enhanced by MPN driver mutations. As priming factors for NLRP3, ROS are notable (Bauernfeind et al., 2011). In MPN, ROS levels are elevated due to cellular stress and ROS overproduction by the malignant clone (Bjørn and Hasselbalch, 2015). ROS-induced damages, such as double-strand DNA breaks, contribute to genomic instability within the HSC niche (Marty et al., 2013). Clonal expansion of the malignant clone is further favored by ROS-induced apoptosis in healthy HSCs, which promotes disease progression (Bjørn and Hasselbalch, 2015). Additionally, to cellular oxidative damages, ROS drive inflammation as priming factors for NLRP3 by promoting its transcriptional upregulation (Bauernfeind et al., 2011;

Kelley et al., 2019). As ROS play a crucial role as inflammasome priming factors and drivers of disease progression it became intriguing to measure their levels in MPN mutated cell lines. This was assessed by measuring ROS production via fluorescence in *JAK2V617F, CALR-del52* and *CALR-ins5* mutated cells. ROS were significantly higher in cells harboring genetic alterations than in the WT control indicating that ROS accumulation is triggered by MPN mutations. Consequently, inflammasome activation can be concluded.

While these findings shed light on the role of spontaneous inflammasome in MPN, it is important to recognize that inflammation in MPN involves multiple players and pathways. Various inflammatory cytokines (e.g., IL-18 and TNFα) contribute to sustaining inflammation (Wang and Zuo, 2019). Also, many other inflammasome activators alongside ROS contribute to inflammasome priming and activation (Tartey and Kannegato, 2019). Therefore, NLRP3 and ROS likely participate among many other stimuli in maintaining inflammation in MPN.

These results prompted an intriguing exploration of how inflammation influences the phenotype of MPN disease. Subsequent in vivo experiments investigated whether the observed inflammatory effects in vitro could be linked to *Nlrp3* deficiency, focusing on fibrosis, MSC loss, and neuropathy.

4.2 *Nlrp3* deficiency in *Jak2*^{VF} mice reduces fibrosis in the BM and spleen and regulates excess megakarypoiesis

Using a MPN mouse model with the most common driver mutation JAK2V617F (*Jak2*^{VF}*)* with a homozygous knock-out in the *Nlrp3* gene, myelofibrosis was assessed by Gordon & Sweet staining of histological slices of the BM and compared with *Jak2*^{VF};*Nlrp3*$^{+/+}$ mice and C57B6 WT mice. Additionally, fibrosis of the spleen, as an organ of extramedullary hematopoiesis, was analyzed. In mice lacking *Nlrp3,* reduction of fibrosis in BM and spleen was observed indicating that the NLRP3 inflammasome plays an indispensable role in the development of fibrosis. In line with these findings another group showed that loss of IL-1β in *Jak2*^{VF} mice reduces myelofibrosis (Rai et al., 2022). That emphasizes that NLRP3 plays a central role in promoting fibrosis in MPN through its regulation of IL-1β production and subsequent NLRP3-mediated inflammatory events (aim 2 as described in chapter 1.5). To analyze whether fibrotic changes could be observed at a transcriptional

level, *COL1A1* messenger RNA (mRNA) expression levels were analyzed. *COL1A1* encodes for Collagen, type I, alpha I, a known marker for fibrosis (Ghosh et al., 2023b). Its expression level in whole BM cells was assessed. RT-qPCR showed that expression of *COL1A1* was significantly lower in *Jak2*^{VF}*;Nlrp3*$^{-/-}$ mice emphasizing that *Nlrp3* has an impact on both the synthesis of RNA and the production of proteins. Further analysis of splenic cells would offer valuable insights into how the observed effects manifest transcriptionally within the spleen. The examination of osteosclerosis, which is also linked with the MPN phenotype, was slightly impacted in the absence of *Nlrp3*, however these changes were not significant. This observation may be attributed to the mouse model used, as evidenced by the *Jak2*^{VF} group displaying minimal osteosclerosis, suggesting that the manifestation of this MPN phenotype could not be adequately observed in this particular model. Consequently, it became challenging to assess the effects of NLRP3 in osteosclerosis within this model context. Still, these results show that *Nlrp3* deficiency reduces fibrosis in the BM and spleen. Koerber et al. demonstrated that inhibiting NLRP3 pharmacologically improves splenomegaly and reduces fibrosis in the BM and spleen in *Jak2*^{VF} mice underscoring the therapeutic promise of NLRP3 blockade in treating MPN (Koerber et al., 2024). However, this data also underscores the involvement of the NLRP inflammasome in development of myelofibrosis in MPN.

Effects on megakaryopioesis were analyzed by H&E staining of BM and spleen sections. Hyperplasia and hypertrophy of megakaryocytes was evident in *Jak2*^{VF} mice and significantly reduced in *Jak2*^{VF} mice lacking *Nlrp3*. These findings are in line with our prior ones showing that the amount of collagen and reticulin fibers is reduced when *Nlrp3* is knocked out. But also, these results show that the NLRP3 inflammasome is crucial for megakaryocytic hyperplasia and involved in progression in myelofibrosis in multiple ways. This is supported by the results of Rai et al., who proved, that *Jak2*^{VF} mice lacking *IL1β* show a reduced number of megakaryocytes in the BM (Rai et al., 2022). Consequently, these findings not only affirm the prevailing notion of IL-1β driving megakaryopoiesis, but also identify NLRP3 as the origin of IL-1β. This is highlighted by the observation that *Nlrp3* deficiency mitigates the effects driven by IL-1β, whereas IL-1β can be activated by other inflammasomes than NLRP3 (Lopez-Casteion and Brough, 2011). IL-1β is recognized for its role in driving megakaryopoiesis, while megakaryocytes, in turn, contribute to myelofibrosis (Rahman et al., 2022; Yang et al., 2017). One potential mechanism for inducing

myelofibrosis involves the release of profibrotic cytokines by megakaryocytes (Gangat and Tefferi, 2020). To determine their fibrotic potential with respect to the NLRP3 inflammasome, it would have been intriguing to connect these data with corresponding levels of TGFβ in the BM and spleen.

Apart from their role in the pathogenesis of myelofibrosis megakaryocytes are essential for thrombopoiesis. Thrombocytosis is one of the clinical symptoms in MPN and accounts for severe complications. Therefore, it can be assumed that *Nlrp3* deficiency suppresses platelet production, but to confirm this hypothesis, measuring of thrombocytes in peripheral blood of mice must be done.

4.3 *Nlrp3* deficiency in *Jak2^{VF}* mice restores nestin^{+} MSCs and sympathetic bone marrow innervation in MPN

Arranz et al. (2014) showed that *Jak2^{VF}* mutant HSCs secrete IL-1β, which damages Schwann cells and sympathetic nerve fibers causing neuropathy. This event results in reduced nestin^{+} MSCs, which regulate normal HSCs and clinically MPN progression (Arranz et al., 2014). To evaluate if IL-1ß dependent neuropathy is driven by NLRP3, changes in the BM microenvironment of *Jak2^{VF}* and *Jak2^{VF};Nlrp3$^{-/-}$* mice were analyzed. Nestin^{+} cells, sympathetic nerve fibers and Schwann cells were stained and counted. Nestin^{+} MSCs are located at different sites of the BM, and therefore nestin^{+} MSCs near vessels, bone trabecula and groups in the BM were assessed. The examination of nestin^{+} endostal niches was hindered by challenges during the IHC staining process, resulting in the loss of bone trabecular margins in certain slides. This led to difficulties in examining the area of interest across all animals, thus affecting the reliability of the results, which showed highest number of nestin^{+} endosteal niches in *Jak2^{VF}* mice. However, nestin^{+} niches and perivascular niches were normalized in *Jak2^{VF};Nlrp3$^{-/-}$* mice and in total, results showed that nestin^{+} MSCs were restored in *Jak2^{VF};Nlrp3$^{-/-}$* mice revealing that the NLRP3 inflammasome is involved in MSC regulation. These results are consistent with the findings of Arranz et al. (2014), indicating a reduction in nestin+ MSCs within the BM of mice expressing the *Jak2^{VF}* mutation. As neuropathy drives MSC loss, sympathetic nerve fibers and Schwann cells in the BM were counted. Results revealed a notable decrease in the quantities of TH^{+} and GFAP^{+} cells in the BM of *Jak2^{VF}* mice compared to the WT group. In *Jak2^{VF}* mice lacking *Nlrp3*, there was an improvement in BM neuropathy, as evidenced

by restoration of sympathetic nerve fibers and Schwann cell numbers to almost normal levels. The deactivated *Nlrp3* signaling in mice was coherent with decreased neuropathy, aligning with the notion that IL-1ß driven impairment of Schwann cells and sympathetic nerve fibers induces neuropathy as demonstrated by Arranz et al. (2014). These findings underscore the significant contribution of the NLRP3 inflammasome to this process.

Having observed robust results at the protein level, it became intriguing to examine whether these findings exhibit consistency at a transcriptional level. Therefore, BM cells were analyzed for mRNA expression level of *Adrb3*, which encodes the β-3-adrenergic receptor. This receptor signaling influences the trafficking of HSCs by modulating the expression of key chemokines in the BM niche, which ultimately impacts the circulation of HSCs in a circadian manner (Méndez-Ferrer et al., 2008). Arranz et al. showed that the absence of β-3-adrenergic receptor accelerated disease development in mice, revealing a protective function of this receptor in the context of MPN (Arranz et al., 2014). In line with the previous results, the expression of *Adrb3* was upregulated in *Jak2*^{VF}*;Nlrp3*$^{-/-}$ mice. This indicates that the IL-1β driven neuropathy is mediated through NLRP3. β-3-sympathomimetic agonists, such as mirabegron, were evaluated in a phase II clinical trial, demonstrating the restoration of nestin^{+} MSCs and a reduction in myelofibrosis (Drexler et al., 2019). This highlights their potential in enhancing therapeutic outcomes within the neuro-hematopoietic axis. As NLRP3 plays a pivotal role within this axis, controlling the inflammasome promises positive effects on neural damages and its consequences. An exciting investigation would be the application of inflammasome inhibitors in MPN and outcome on neuroglial damage and MSC survival. Overall, these results support the hypothesis that IL-1β dependent neuroglial damage is largely driven by NLRP3.

4.4 Limitations and outlook

This study investigated the role of the NLRP3 inflammasome in bone marrow fibrosis, neural damage, and MSC survival in MPN. While the results highlight the contribution of NLRP3, limitations and future directions warrant attention.

The findings demonstrate that spontaneous inflammasome activity is increased in MPN; however, the exact contribution of NLRP3 activation in these processes remains unclear. Therefore, it would be particularly interesting to explore the specific role of NLRP3 in driving inflammation in MPN, as understanding its contribution could offer valuable insights into potential therapeutic strategies. Future work should aim to analyze the range of inflammasome-related pathways and regulators, including transcription factors and other cytokines such as TNFα, IL-6, and IL-18.

Pharmacological inhibition of NLRP3 has emerged a promising therapeutic strategy. First small molecule inhibitors targeting NLRP3 like MCC950 showed strong efficacy in preclinical inflammation models (Coll et al., 2015), and newer compounds have entered clinical trials for immune-mediated diseases (Li et al., 2023). Currently, the small molecule NLRP3 inhibitor DFV890 is being tested in a Phase 1b trial in patients with Myelodysplastic Syndromes (MDS) and Chronic Myelomonocytic Leukemia (CMML) (Garcia-Manero et al., 2024). In the same *Jak2*^{VF} mouse model used in this study, pharmacological blockade of NLRP3 using the inhibitor IFM-2384 reduced splenomegaly, thrombocytosis and BM fibrosis (Koerber et al., 2024), supporting the translational potential of pharmacological targeting NLRP3 in MPN.

Although the study revealed reduced BM and splenic fibrosis in *Jak2*^{VF}*;Nlrp3*$^{-/-}$ mice, the observed changes in osteosclerosis were not significant, limiting the ability to draw definitive conclusions about the role of NLRP3 in this aspect of MPN pathology. Additionally, the study relied on established fibrosis markers, which may not fully capture the dynamics of fibrotic processes. Future investigations should leverage advanced molecular and imaging techniques to assess fibrosis progression in long-term disease models. Moreover, exploring the efficacy of inflammasome inhibitors at later disease stages could provide critical insights into their therapeutic potential for managing advanced myelofibrosis. Regarding neuropathy, *Nlrp3* deficiency alleviated neuroglial damage and improved MSC survival, but the exact mechanisms linking the inflammatory microenvironment to neurodegeneration in MPN remain unresolved. Future studies should delve into the cross-talk

between immune cells, neural components, and the hematopoietic niche. Additionally, long-term studies assessing MSC functionality and their regenerative potential in *Nlrp3*-deficient mice could help clarify the full scope of the inflammasome's influence on neuroglial health. Trials with inflammasome inhibitors targeting neuroglial damage may also offer promising therapeutic directions.

This study provides valuable insights into the role of NLRP3 in MPN. However, further investigation is required to comprehensively map the inflammatory pathways involved, clarify the molecular mechanisms underpinning fibrotic progression, and understand the interactions between inflammation and neuroglial damage. These insights will be crucial for developing targeted and effective therapies to improve patient outcomes.

5 Summary

Inflammation is a defining feature of BCR-ABL-negative Myeloproliferative Neoplasms (MPN). The driver mutations in *JAK2*, *CALR*, and *MPL* activate JAK-STAT signaling, promoting the expansion of the malignant clone and triggering an inflammatory response. The resulting elevation of inflammatory cytokines in the bone marrow microenvironment is thought to play a crucial role in initiating and advancing the disease. A key effector cytokine in this process is IL-1β, which contributes to critical disease-related events, including myelofibrosis, bone marrow (BM) neuropathy, and the reduction of mesenchymal stem cells. The NLRP3 inflammasome is central to the regulation of IL-1β production.

The objective of this thesis was to investigate the role of the NLRP3 inflammasome in IL-1β-dependent bone marrow fibrosis, neural damage and mesenchymal stem cell (MSC) survival in MPN. To achieve this goal, three main objectives were pursued.

The first aim examined whether BCR-ABL-negative MPN cell lines exhibit signs of inflammation (see chapter 1.5). Murine cell lines expressing *Jak2V617F*, *CALR-del52*, or *CALR-ins5* were used for this analysis. Inflammation was assessed by measuring active Caspase-1 and ROS production, which are indicators of inflammasome activity and priming. The results revealed increased levels of both Caspase-1 and ROS in cell lines harboring MPN driver mutations.

The second aim investigated whether *Nlrp3* deficiency results in reduced BM fibrosis and normalization of megakaryopoiesis in MPN (see chapter 1.5). A murine *Jak2*^{VF} MPN model was utilized, comparing wildtype *Nlrp3* and homozygous *Nlrp3* knockout mice. Reticulin and collagen fiber staining (Gordon & Sweet) was performed on BM and spleen sections to assess fibrosis, and osteosclerosis was evaluated by H&E staining. Expression levels of *COL1A1*, a gene associated with fibrosis, were measured by RT-qPCR. The megakaryocyte size and count were determined in the BM and spleen and scoring of fibrosis in both BM and spleen showed less pronounced fibrosis in *Nlrp3*-deficient mice. While osteosclerosis displayed a similar trend, the results did not reach statistical significance. *COL1A1* expression was downregulated in *Jak2*^{VF}*;Nlrp3*$^{-/-}$ mice compared to *Jak2*^{VF} mice, and megakaryocyte hyperplasia and hypertrophy were normalized in *Jak2*^{VF}*;Nlrp3*$^{-/-}$ mice

The third aim focused on assessing whether *Nlrp3* deficiency reduces damage to neuroglial cells and enhances MSC survival (see chapter 1.5). The same *Jak2*^{VF} mouse model

was used. Neuropathy was evaluated by staining BM sections for sympathetic nerve fibers and Schwann cells, and MSC survival was assessed by MSC staining. Additionally, the expression of β3-adrenergic receptor (*Adrb3*) was analyzed by RT-qPCR. Quantitative analysis revealed that neuropathy was significantly ameliorated in *Jak2*^{VF}*;Nlrp3*$^{-/-}$ mice compared to *Jak2*^{VF} mice. Furthermore, MSC loss was less severe in this group, and *Adrb3* expression was upregulated in *Jak2*^{VF}*;Nlrp3*$^{-/-}$ mice compared to *Jak2VF* mice.
The results of this study contribute to a deeper understanding of the impact of the NLRP3 inflammasome in MPN. Further research is needed to evaluate the therapeutic potential of inflammasome inhibitors, as they hold promise for improving treatment outcomes in MPN.

6 List of figures

7 List of tables

8 References

Anderson LA, McMullin MF. Epidemiology of MPN: What Do We Know? Curr Hematol Malig Rep 2014; 9: 340–349

Arranz L, Sánchez-Aguilera A, Martín-Pérez D, Isern J, Langa X, Tzankov A, et al. Neuropathy of haematopoietic stem cell niche is essential for myeloproliferative neoplasms. Nature 2014; 512: 78–81

Bader MS, Meyer SC. JAK2 in Myeloproliferative Neoplasms: Still a Protagonist. Pharmaceuticals (Basel) 2022; 15: 160

Bauernfeind F, Bartok E, Rieger A, Franchi L, Núñez G, Hornung V. Cutting edge: reactive oxygen species inhibitors block priming, but not activation, of the NLRP3 inflammasome. J Immunol 2011; 187: 613–617

Baumeister J, Chatain N, Sofias AM, Lammers T, Koschmieder S. Progression of Myeloproliferative Neoplasms (MPN): Diagnostic and Therapeutic Perspectives. Cells 2021; 10: 3551

Behrmann L, Wellbrock J, Fiedler W. The bone marrow stromal niche: a therapeutic target of hematological myeloid malignancies. Expert Opin Ther Targets 2020; 24

Bjørn ME, Hasselbalch HC. The Role of Reactive Oxygen Species in Myelofibrosis and Related Neoplasms. Mediators Inflamm 2015; 2015: 648090

Blevins HM, Xu Y, Biby S, Zhang S. The NLRP3 Inflammasome Pathway: A Review of Mechanisms and Inhibitors for the Treatment of Inflammatory Diseases. Front Aging Neurosci 2022; 14: 879021

Chaplin DD. Overview of the Immune Response. J Allergy Clin Immunol 2010; 125: 3-23

Coll R, Robertson A, Chae J, Higgins S, Munoz-Planillo R, Inserra MC, et al. A small-melcule inhibitor of the NLARP3 inflammasome for the treatment of inflammatory diseases. Nat Med 2015; 21: 248-255

Curto-Garcia N, Harrison C, McLornan DP. Bone marrow niche dysregulation in myeloproliferative neoplasms. Haematologica 2020; 105: 1189–1200

Drexler B, Passweg JR, Tzankov A, Bigler M, Theocharides AP, Cantoni N, et al. The sympathomimetic agonist mirabegron did not lower JAK2-V617F allele burden, but restored nestin-positive cells and reduced reticulin fibrosis in patients with myeloproliferative neoplasms: results of phase II study SAKK 33/14. Haematologica 2019; 104: 710–716

Fernández KS, de Alarcón PA. Development of the Hematopoietic System and Disorders of Hematopoiesis that Present During Infancy and Early Childhood. Pediatr Clin North Am 2013; 60: 1273–1289

Gangat N, Tefferi A. Myelofibrosis biology and contemporary management. Br J Haematol 2020; 191: 152–170

García-García A, de Castillejo CLF, Méndez-Ferrer S. BMSCs and hematopoiesis. Immunol Lett 2015; 168: 129–135

Garcia-Manero G, Abaza Y, Greenberg PL, Haque T, Velázquez Kennedy K, Della Porta MG, et al. Preliminary Safety and Biomarker Results of the NLRP3 Inflammasome Inhibitor DFV890 in Adult Patients with Myeloid Diseases: A Phase 1b Study. Blood 2024; 144 (Supplement 1): 353

Ghosh Kanjaksha, Shome DK, Kulkarni B, Ghosh MK, Ghosh Kinjalka. Fibrosis and bone marrow: understanding causation and pathobiology. J Transl Med 2023; 21: 703

Harrison C, Kiladjian J-J, Al-Ali HK, Gisslinger H, Waltzman R, Stalbovskaya V, et al. JAK Inhibition with Ruxolitinib versus Best Available Therapy for Myelofibrosis. N Engl J Med 2012; 366: 787–798

Harrison CN, Vannucchi AM, Kiladjian J-J, Al-Ali HK, Gisslinger H, Knoops L, et al. Long-term findings from COMFORT-II, a phase 3 study of ruxolitinib vs best available therapy for myelofibrosis. Leukemia 2016; 30: 1701–1707

Hasan S, Lacout C, Marty C, Cuingnet M, Solary E, Vainchenker W, et al. JAK2V617F expression in mice amplifies early hematopoietic cells and gives them a competitive advantage that is hampered by IFNα. Blood 2013; 122: 1464–1477

Hobbie K, Elmore SA, Kolenda-Roberts HM. 2014. Spleen−Fibrosis. In: Cesta MF, Herbert RA, Brix A, Malarkey DE, Sills RC (Eds..), National Toxicology Program Nonneoplastic Lesion Atlas. Available: https://ntp.niehs.nih.gov/nnl/immune/spleen/fibrosis/index.htm [accessed 01. February 2025]

Hoffman R, Prchal JT, Samuelson S, Ciurea SO, Rondelli D. Philadelphia Chromosome–Negative Myeloproliferative Disorders: Biology and Treatment. Biol Blood Marrow Transplant 2007; 13: 64–72

Kelley N, Jeltema D, Duan Y, He Y. The NLRP3 Inflammasome: An Overview of Mechanisms of Activation and Regulation. Int J Mol Sci 2019; 20: 3328

Khoury JD, Solary E, Abla O, Akkari Y, Alaggio R, Apperley JF, et al. The 5th edition of the World Health Organization Classification of Haematolymphoid Tumours: Myeloid and Histiocytic/Dendritic Neoplasms. Leukemia 2022; 36: 1703–1719

Kim CH. Homeostatic and pathogenic extramedullary hematopoiesis. J Blood Med 2010; 1: 13–19

Kim SY, Im K, Park SN, Kwon J, Kim J-A, Lee DS. CALR, JAK2, and MPL mutation profiles in patients with four different subtypes of myeloproliferative neoplasms: primary myelofibrosis, essential thrombocythemia, polycythemia vera, and myeloproliferative neoplasm, unclassifiable. Am J Clin Pathol 2015; 143: 635–644

Klampfl T, Gisslinger H, Harutyunyan AS, Nivarthi H, Rumi E, Milosevic JD, et al. Somatic Mutations of Calreticulin in Myeloproliferative Neoplasms. N Engl J Med 2013; 369: 2379–2390

Kleppe M, Kwak M, Koppikar P, Riester M, Keller M, Bastian L, et al. JAK–STAT Pathway Activation in Malignant and Nonmalignant Cells Contributes to MPN Pathogenesis and Therapeutic Response. Cancer Discov 2015; 5: 316–331

Koerber R-M, Krollmann C, Cieslak K, Tregel E, Brümmendorf TH, Koschmieder S, et al. NLRP3-induced systemic inflammation controls the development of JAK2V617F mutant myeloproliferative neoplasms. bioRxiv 2024: 2024.03.09.583936

Korn C, Méndez-Ferrer S. Myeloid malignancies and the microenvironment. Blood 2017;

129: 811–822

Koschmieder S, Mughal TI, Hasselbalch HC, Barosi G, Valent P, Kiladjian J-J, et al. Myeloproliferative neoplasms and inflammation: whether to target the malignant clone or the inflammatory process or both. Leukemia 2016; 30: 1018–1024

Kröger NM, Deeg JH, Olavarria E, Niederwieser D, Bacigalupo A, Barbui T, et al. Indication and management of allogeneic stem cell transplantation in primary myelofibrosis: a consensus process by an EBMT/ELN international working group. Leukemia 2015; 29: 2126–2133

Kurzrock R, Kantarjian HM, Druker BJ, Talpaz M. Philadelphia ChromosomePositive Leukemias: From Basic Mechanisms to Molecular Therapeutics. Ann Intern Med 2003; 138: 819–830

Kvasnicka HM. The differential diagnosis of classical myeloproliferative neoplasms (MPN): the updated WHO criteria. Rinsho Ketsueki 2019; 60: 1166–1175

Kvasnicka HM, Beham-Schmid C, Bob R, Dirnhofer S, Hussein K, Kreipe H, et al. Problems and pitfalls in grading of bone marrow fibrosis, collagen deposition and osteosclerosis - a consensus-based study. Histopathology 2016; 68: 905–915

Langabeer SE. Chasing down the triple-negative myeloproliferative neoplasms: Implications for molecular diagnostics. JAKSTAT 2016; 5: e1248011

Leimkühler NB, Gleitz HFE, Ronghui L, Snoeren IAM, Fuchs SNR, Nagai JS, et al. Heterogeneous bone-marrow stromal progenitors drive myelofibrosis via a druggable alarmin axis. Cell Stem Cell 2021; 28: 637-652.e8

Li N, Zhang R, Tang M, Zhao M, Jiang X, Cai X et al. Recent Progress and Prospects of Small Molecules for NLRP3 Inflammasome Inhibition. J Med Chem 2023; 66 (21): 14447-14473

Lopez-Castejon G, Brough D. Understanding the mechanism of IL-1β secretion. Cytokine Growth Factor Rev 2011; 22: 189–195

Lucas D. Structural organization of the bone marrow and its role in hematopoiesis. Curr

Opin Hematol 2021; 28: 36

Martinon F, Tschopp J. Inflammatory caspases and inflammasomes: master switches of inflammation. Cell Death Differ 2007; 14: 10–22

Marty C, Lacout C, Droin N, Le Couédic J-P, Ribrag V, Solary E, et al. A role for reactive oxygen species in JAK2V617F myeloproliferative neoplasm progression. Leukemia 2013; 27: 2187–2195

Méndez-Ferrer S, Lucas D, Battista M, Frenette PS. Haematopoietic stem cell release is regulated by circadian oscillations. Nature 2008; 452: 442–447

Moossavi M, Parsamanesh N, Bahrami A, Atkin SL, Sahebkar A. Role of the NLRP3 inflammasome in cancer. Mol Cancer 2018; 17: 158

Morcos MNF, Li C, Munz CM, Greco A, Dressel N, Reinhardt S, et al. Fate mapping of hematopoietic stem cells reveals two pathways of native thrombopoiesis. Nat Commun 2022; 13: 4504

Parciante E, Cumbo C, Anelli L, Zagaria A, Redavid I, Minervini A, et al. The Role of NLRP3, a Star of Excellence in Myeloproliferative Neoplasms. Int J Mol Sci 2023; 24: 4860

Pizzi M, Croci GA, Ruggeri M, Tabano S, Dei Tos AP, Sabattini E, et al. The Classification of Myeloproliferative Neoplasms: Rationale, Historical Background and Future Perspectives with Focus on Unclassifiable Cases. Cancers (Basel) 2021; 13: 5666

Pucella JN, Upadhaya S, Reizis B. The Source and Dynamics of Adult Hematopoiesis: Insights from Lineage Tracing. Annu Rev Cell Dev Biol 2020; 36: 529–550

Quintás-Cardama A, Abdel-Wahab O, Manshouri T, Kilpivaara O, Cortes J, Roupie A-L, et al. Molecular analysis of patients with polycythemia vera or essential thrombocythemia receiving pegylated interferon α-2a. Blood 2013; 122: 893–901

Rahman MF-U, Yang Y, Le BT, Dutta A, Posyniak J, Faughnan P, et al. Interleukin-1 contributes to clonal expansion and progression of bone marrow fibrosis in JAK2V617F-induced myeloproliferative neoplasm. Nat Commun 2022; 13: 5347

Rai S, Grockowiak E, Hansen N, Luque Paz D, Stoll CB, Hao-Shen H, et al. Inhibition of

interleukin-1β reduces myelofibrosis and osteosclerosis in mice with JAK2-V617F driven myeloproliferative neoplasm. Nat Commun 2022; 13: 5346

Ratajczak MZ, Bujko K, Cymer M, Thapa A, Adamiak M, Ratajczak J, et al. The Nlrp3 inflammasome as a “rising star” in studies of normal and malignant hematopoiesis. Leukemia 2020; 34: 1512–1523

Schepers K, Campbell TB, Passegué E. Normal and Leukemic Stem Cell Niches: Insights and Therapeutic Opportunities. Cell Stem Cell 2015; 16: 254–267

Schepers K, Pietras EM, Reynaud D, Flach J, Binnewies M, Garg T, et al. Myeloproliferative Neoplasia Remodels the Endosteal Bone Marrow Niche into a Self-Reinforcing Leukemic Niche. Cell Stem Cell 2013; 13: 285–299

Scherber R, Dueck AC, Johansson P, Barbui T, Barosi G, Vannucchi AM, et al. The Myeloproliferative Neoplasm Symptom Assessment Form (MPN-SAF): International Prospective Validation and Reliability Trial in 402 patients. Blood 2011; 118: 401–408

Stegelmann F, Teichmann LL, Heidel FH, Crodel CC, Ernst T, Kreil S, et al. Clinicohematologic and molecular response of essential thrombocythemia patients treated with pegylated interferon-α: a multi-center study of the German Study Group-Myeloproliferative Neoplasms (GSG-MPN). Leukemia 2023; 37: 924–928

Szybinski J, Meyer SC. Genetics of Myeloproliferative Neoplasms. Hematol Oncol Clin North Am 2021; 35: 217–236

Tallarico M, Odenike O. Secondary Acute Myeloid Leukemias Arising From Philadelphia Chromosome Negative Myeloproliferative Neoplasms: Pathogenesis, Risk Factors, and Therapeutic Strategies. Curr Hematol Malig Rep 2015; 10: 112–117

Tartey S, Kanneganti T-D. Differential role of the NLRP3 inflammasome in infection and tumorigenesis. Immunology 2019; 156: 329–338

Tavian M, Biasch K, Sinka L, Vallet J, Péault B. Embryonic origin of human hematopoiesis. Int J Dev Biol 2010; 54: 1061–1065

Tefferi A. Primary myelofibrosis: 2023 update on diagnosis, risk-stratification, and management. Am J Hematol 2023; 98: 801–821

Tefferi A. Novel mutations and their functional and clinical relevance in myeloproliferative neoplasms: JAK2, MPL, TET2, ASXL1, CBL, IDH and IKZF1. Leukemia 2010; 24: 1128–1138

Tefferi A, Guglielmelli P, Larson DR, Finke C, Wassie EA, Pieri L, et al. Long-term survival and blast transformation in molecularly annotated essential thrombocythemia, polycythemia vera, and myelofibrosis. Blood 2014; 124: 2507–2513

Wang Y, Zuo X. Cytokines frequently implicated in myeloproliferative neoplasms. Cytokine 2019; 1: 100005

Yang M, Li S, Zhang X, Cao R, Li C, Chong BH. Pro-Inflammatory Cytokine IL-1b on Megakaryopoiesis: A Possible Explanation of Thrombocytosis in Inflammation. Blood 2017; 130: 4851

Zhang Y, Gao S, Xia J, Liu F. Hematopoietic Hierarchy – An Updated Roadmap. Trends Cell Biol 2018; 28: 976–986

Zoi K, Cross N. Genomics of myeloproliferative neoplasms. J Clin Oncol 2017; 35: 947–954

Zon LI. Intrinsic and extrinsic control of haematopoietic stem-cell self-renewal. Nature 2008; 453: 306–313

9 Statement on personal contributions

With regard to my doctoral thesis, I declare the following: The overall research concept and study design were developed in collaboration with my supervisors. I personally carried out the data collection, analysis, and interpretation of the results presented in this thesis. The mouse model and cell lines used had been previously established (as described in the Methods section). In line with the current statement of the German Research Foundation (DFG) on generative AI models, I further declare that generative language models were used exclusively for linguistic refinement. The scientific content, data analysis, and conclusions are entirely my own and were not influenced by such tools.

10 Publications

The data presented in the Results section have been partially published previously:

Koerber R-M, Krollmann C, Cieslak K, **Tregel E**, Brümmendorf TH, Koschmieder S, et al. NLRP3-induced systemic inflammation controls the development of JAK2V617F mutant myeloproliferative neoplasms. bioRxiv 2024: 2024.03.09.583936

11 Acknowledgments

I would like to sincerely thank Professor Brossart for giving me the opportunity to conduct my doctoral research in his clinic. This opportunity enabled me to gather very valuable experiences in this field of research and has enriched my academic growth in many ways.

My gratitude also goes to Dr. Lino Teichmann for his guidance throughout the project. His support in structuring the research and providing scientific advice was invaluable. His insights and support were also essential in refining and presenting the outcomes of this work.

I would like to extend my deepest thank you to Dr. Miriam Körber, for her unwavering support throughout this project. Her assistance and continuous encouragement, played a crucial role in the successful completion of this research.

I am also grateful for the support I received in securing funding through the EKFS Neuro-Immunology program. I would like to specifically thank Dr. Lino Teichmann and Dr. Miriam Körber for their invaluable help during the application process and for their guidance in ensuring the successful implementation of this project.

I would also like to acknowledge the members of the AG Teichmann / AG Baumjohann, particularly Kevin Cieslak, Dr. Calvin Krollmann, and Luisa Bach, for their expertise and collaboration. Their guidance in laboratory techniques and their team spirit made working in the lab both productive and enjoyable. The time spent with our "office group" remains one of the highlights of this journey.

Additionally, I extend my thanks to all colleagues at BMZ I and II, whose collaboration and assistance made it possible to conduct the experiments essential to this project.

Finally, I am deeply grateful to my family and friends for their unwavering support and encouragement, which have been a constant source of strength and motivation throughout this process.